공학박사학위논문

스팀 생산 히트펌프의 성능 향상 및 동적 거동에 대한 연구

The performance improvement and dynamic behavior of steam generation heat pump

2020 년 2 월

서울대학교 대학원

기계항공공학부

강 대 훈

스팀 생산 히트펌프의 성능 향상 및 동적 거동에 대한 연구

The performance improvement and dynamic behavior of steam generation heat pump

지도교수 김 민 수

이 논문을 공학박사 학위논문으로 제출함

2019 년 10 월

서울대학교 대학원

기계항공공학부

강 대 훈

강대훈의 공학박사 학위논문을 인준함

2019 년 12 월

위 원 장 : 민 경 덕

부위원장 : 김 민 수

위 원 : 송 한 호

위 원 : 도 형 록

위 원 : 장 영 수

Abstract

The performance improvement and dynamic behavior of steam generation heat pump

Dae Hoon Kang
Department of Mechanical and Aerospace Engineering
The Graduate School
Seoul National University

Recently, reduction of energy consumption is required by international environmental regulation due to global warming. The industrial sector accounts for a large share of energy consumption in the case of manufacturing-oriented countries, and industrial heat generation is especially important. The introduction of the heat pump is considered as a means of steam generation and recovering unutilized heat, which requires cooling before discharging. New refrigerants with high critical temperature made it possible to generate steam beyond hot water production. Heat pumps are capable of more heat generation and recovery of low-temperature heat source from the same primary energy than conventional boilers.

However, studies on heat pumps capable of making steam with a high

temperature over 100 degrees is in early stage. Existing studies have searched for the types of refrigerants that can operate at high temperatures and compared the system configurations. As a system configuration, the application of an internal heat exchanger shows high performance. However, the study of the change of the configuration of the internal heat exchanger and the study of the combination of the flash tank are limited.

Therefore, in this study, the design and dynamic characteristics of the steam generation heat pump were considered in generally expected operating conditions. For this purpose, an analytical study was conducted prior to the experimental study, and a method to simulate the change of the configuration of the internal heat exchanger was explored and an experimental study was conducted.

Through experiments, the direction of the performance improvement of the steam production heat pump was suggested, and the influence of each control variable on the heating capacity and system performance was analyzed. Bypass line was used to change the mass flow rate of the internal heat exchanger, and the change of heat capacity and the total mass flow rate were observed. This method can change the evaporating pressure and the refrigerant mass flow rate in addition to the expansion valve.

In addition, unlike hot water generation, which was previously possible at atmospheric pressure, the generation of steam and the pressure of the tank have a close influence on the behavior of the heat pump. Also, the system

characteristics differ from each start-up stage. Therefore, in this study, a dynamic model was proposed by analyzing the transient-state characteristics change of flash tank considering heat pump under start-up condition and verified with the experimental results.

Such a study is expected to be helpful in analyzing the behavior in the study of a steam generation heat pump with a flash tank, and is expected to reduce energy consumption in industrial field.

Keyword: Heat pump, Flash tank, Steam, Heat exchanger, Waste heat recovery

***Identification Number*: 2014-21570**

Contents

List of Figure

List of Tables

Nomenclature

CFC	Chlorofluoro-carbon
COP	Coefficient of performance
DSC	Degree of subcooled
DSG	Direct steam generation
DSH	Degree of superheat
EEV	Electric expansion valve
FEM	Finite element method
FT	Flash tank
GWP	Global warming potential
HFO	Hydrofluoroolefin
HRSG	Heat recovery steam generation
htc	heat transfer coefficient (local)
IHX	Internal heat exchanger
MVR	Mechanical vapor compression
NPSH	Net positive suction head
ODP	Ozone depletion potential
ORC	Organic rankine cycle
PID	Proportional, Integral, Differential
RO	Reverse osmosis
SGHP	Steam generation heat pump
VI	Vapor injection
WWSHP	Wastewater source heat pump

Greek

η	Efficiency
τ	Time constant
ε	Effectiveness of the heat exchanger

Subscript

comp	Compressor
con	Condenser
d	Differential
eva	Evaporator
f	Friction loss
FT	Flash tank
i	Integral
ihx	Internal heat exchanger
p	Pump, Proportional
ref	Refrigerant
s	surface
v	Vapor
wat	Water

Chapter 1. Introduction

1.1 Background of the study

To reduce CO_2 emissions and restrain global warming, many countries have agreed to tighten up international environmental regulations at international conventions such as COP21 [1]. To solve this urgent task related to our planet and satisfy these regulations, energy saving technologies must be developed and applied in many industrial fields. Energy usage in the industry sector has accounted for a substantial amount of total energy consumption; 32% in the USA [2]. Therefore, saving energy in the industrial field could be the main focus in responding to environmental regulations, and becomes an urgent task to solve.

Steam is a naturally benign fluid which is widely used in many industrial fields because of its stability, compatibility, sustainability, especially because of stable heat exchange by latent heat. About 45% of the energy consumption in the industrial field is used to generate steam [3]. Energy for steam generation corresponds to 10% of the total energy consumption of humanity, and half of the energy consumption in the power generation sector. By this reason, various technologies are developed to lower the energy usage for the steam generation.

Steam generation heat pump (SGHP) is getting considerable attention to make high-temperature steam from a rather low-temperature water in a way to recover waste heat. Conventional heat pumps are mainly used for heating air or water. Unlikely, steam generation heat pump recovers waste heat from diverse industrial processes and produces steam which has high potential to be used in heating, drying, sterilization, and humidification. Figure 1.1 and 1.2 show the position of the SGHP. SGHP is proposed to pursue those two objectives.

The heat pump has an advantage in steam production. Conventional steam generation methods include boiler, heat recovery steam generation (HRSG), and solar direct steam generation (DSG). A heat pump can supply higher amounts of heat with the same primary energy input than a boiler, as shown in Figure 1.3. The heat pump is much useful method compared with steam generation using a boiler in a sense that the thermodynamic usefulness is enhanced when temperature lift is reduced. HRSG focuses on utilizing high-temperature heat source, unlike heat pump recovering lower heat source, and steam produced through HRSG is mainly used for electricity production by a steam turbine in a power plant. Solar DSG is environmentally friendly but has low heat recovery density. Recently, the connection between solar DSG and a boiler or heat pump is getting lots of attention [4, 5].

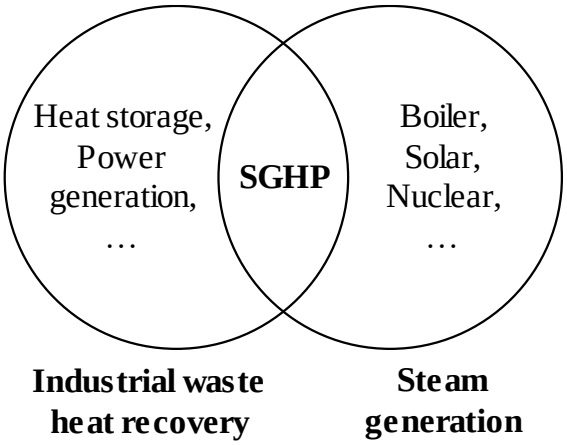

Fig. 1.1 Position of the steam generation heat pump

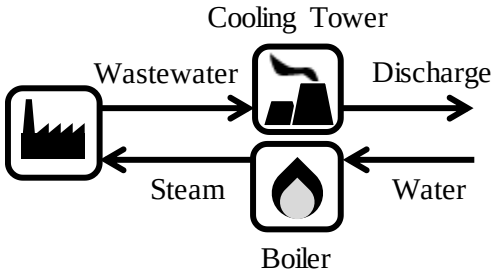

(a) Conventional steam generation by boiler and cooling tower

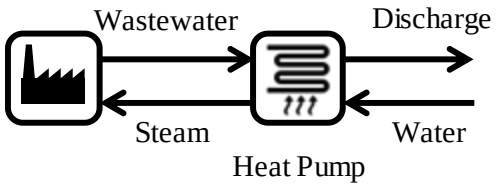

(b) Steam generation and cooling by heat pump

Fig. 1.2 Comparison between conventional and newly suggested system

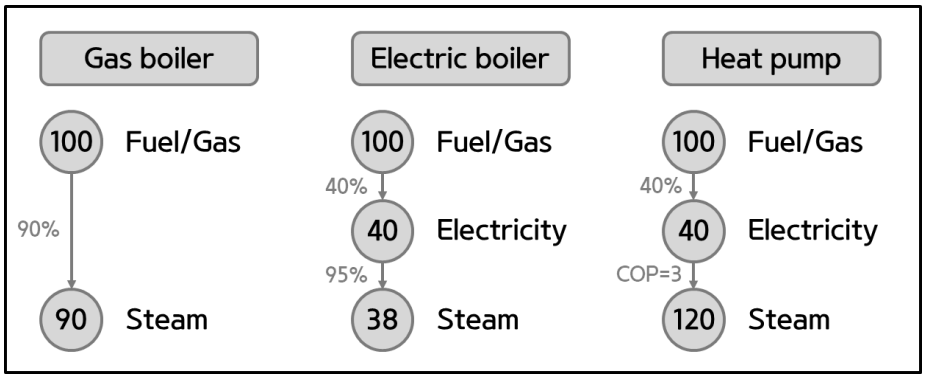

Fig. 1.3 An example of the energy usage for steam generation

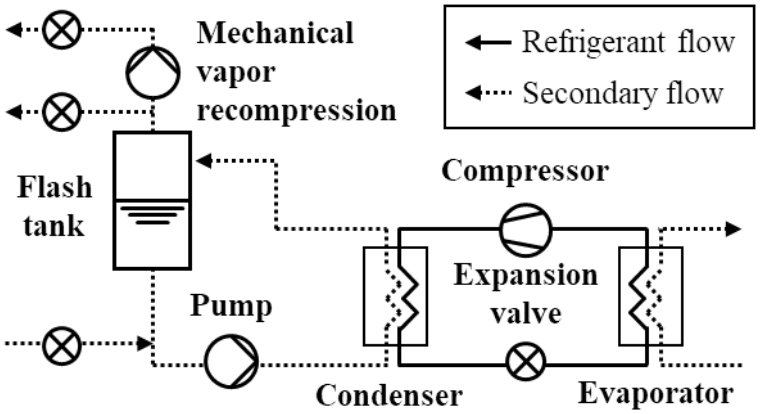

Fig. 1.4 Schematic diagram of commercialized SGHP

Initial research on steam generation heat pumps was conducted by KOBELCO (Kobe steel) and CRIEPI (the electric power company of Japan), who first released a commercialized steam generation heat pump [6, 7]. The schematic diagram is shown in Figure 1.4. The SGH120 model showed a COP of 3.5 at a temperature of 65~120℃ by heat pump applying a two-stage twin-screw compressor. They also released the SGH165 model, which involves the addition of the MVR (mechanical vapor recompression) to the SGH120 to achieve a higher temperature.

On the other hand, in Europe, EDF (the electric power company of France) gathered institutions such as Danfoss, CIAT, DTI and Johnson control, and launched an 'ALTER ECO project' and built pilot plant in 2012 [8]. The pilot plant of EDF achieved a COP of 3 to 4 for 60 to 120℃ and COP of 1 to 2 for 60~140℃.

In general, boilers with a capacity of less than 30 ton per hour are manufactured and sold in a packaged unit system, and larger capacity boilers are assembled in the field. A boiler of 0.1 ton per hour is also called a mini boiler. Heat demand for steam in textile, dyeing, food, and paper industry is less than 10 ton per hour, and chemical, metal processing plant requires more steam generation rate. Commercialized steam generation heat pump produces 0.5 to 0.9 ton per hour of steam. It can be applied in the form of a small scale, sold as a unit model, and installed at the field.

1.2 Literature survey

1.2.1 Industrial low-grade waste heat recovery

The literature on industrial heat demand and amount of un-utilized thermal energy are as follows. In industrial fields, steam or hot water is used as a medium of heat exchange. Hot water and steam are used to be heat source and also used by themselves, and steam is preferred for constant heat exchange by a large latent heat capacity. Lauterbach [9] summarized that industrial heat demand by boiling water under 100℃ and steam under 200℃ is similar in Germany. Bobelin [10] shows demands of heat under 140℃ in the French industrial sector. Accordingly, energy-saving methods for the steam generation process will significantly contribute to reducing industrial energy consumption. Miró et al. [11] summarized the amount of worldwide industrial waste heat potential by the country and the industry. Its amount showed a similar tendency to energy consumption amount. Zhang et al. [12] also showed that industrial waste heat amount in a specific country is enormous. The authors showed that the amount of waste heat in the industrial field differs depending on each country's specialized industrial sector.

Recovering waste heat makes it possible to remove the cooling tower, which should operate when discharging hot wastewater to the environment. The literature on the types of technologies for heat recovery is as follows. Brückner

et al. [13] categorized and listed the methods of recovering industrial waste heat, as shown in Figure 1.5. Also, the temperature range of waste heat source from various processes and the required temperature range of various processes are listed. Steam generation heat pump can be summarized to WHTH (waste heat to heat). Broberg et al. [14] showed that the recovery of waste heat (WHTH) is better than power generation (WHTP, waste heat to power) because of its potential amount and CO_2 reduction, and various heat recovery methods are suggested. Harvesting, storage, utilization (district heating and cooling, heat cooperation), and conversion (Rankine cycle, thermoelectric generator, thermo-photovoltaic, Stirling engine, phase change material engine). Huang et al. [15] summarized a case study of industrial waste heat recovery in Asia, and also listed heat utilization technologies Such as heat pump, heat pipe, boiler, power generation, and heat storage.

Among the heat recovery technologies in the industry, the researches on heat pumps are as follows. Heat pump technologies program (HPC) under the International Energy Agency (IEA) [16] has researched to recover heat by a heat pump steadily. Zhang et al. [12] categorized heat pump technologies into refrigerants, cycles, components, and applications, and classified as vapor compression type, absorption type, and chemical type. Figure 1.6 shows an itemization of heat pump system technologies.

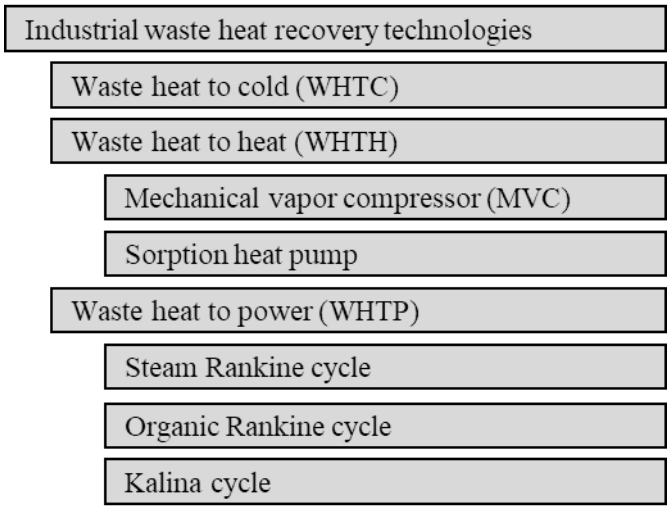

Fig. 1.5 Methods of recovering industrial waste heat

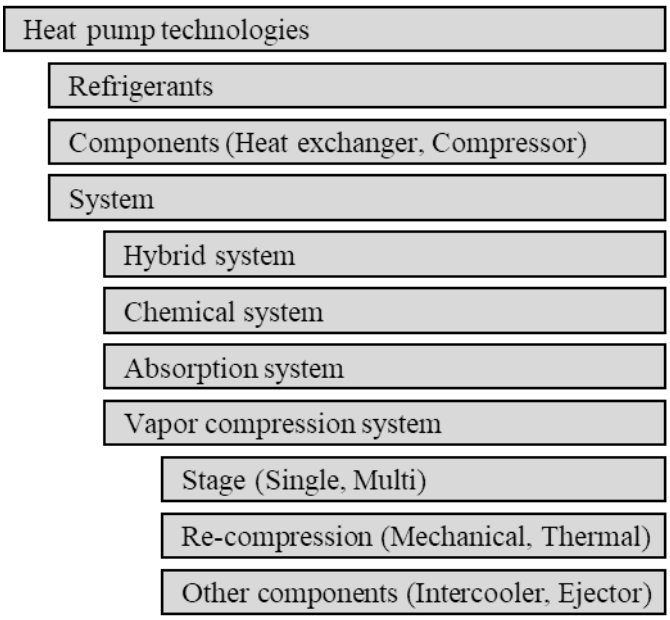

Fig. 1.6 Itemization of heat pump technologies

Wang et al. [17] investigated various literature on recovering a low-temperature heat source by a heat pump. Through the analysis, the refrigerant and the cycle according to the temperature range were matched, as shown in Figure 1.7. At the high-temperature range, vapor injection cycle, two-stage compression cycle, and single cycle are recommended. Culha et al. [18] summarized the refrigerant, capacity, COP, heat exchanger, performance assessment of wastewater source heat pump (WWSHP). The authors considered system configuration, heat exchanger, and control strategy as key variables and reviewed them with detailed drawings. Hepbasli et al. [19] studied heat exchangers were key variables of WWSHP, and the authors categorized the type of heat exchangers by the use as domestic, sewage, and treatment.

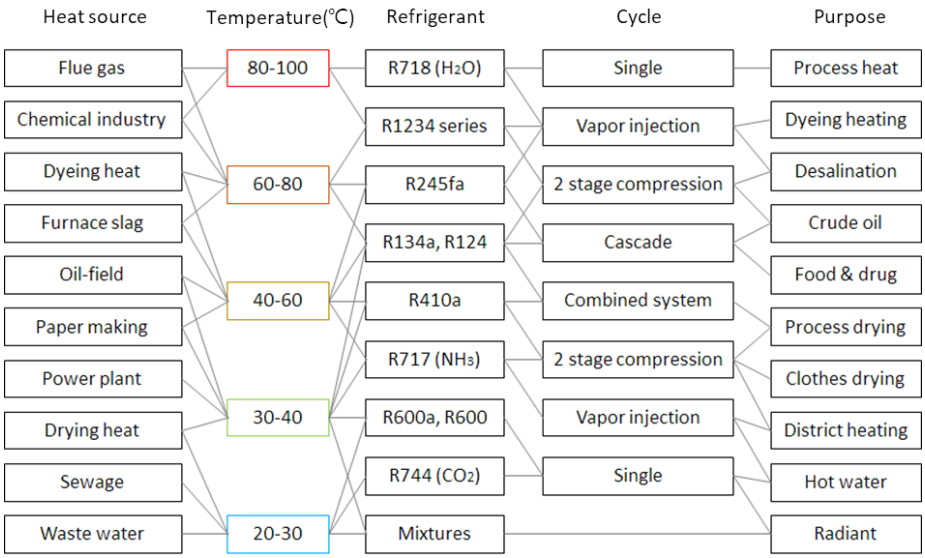

Fig. 1.7 A guideline for compression heat pump with waste heat recovery

1.2.2 High-temperature heat pump

Research to raise the temperature to higher than 100℃ using an absorption heat pump and a chemical heat pump is in an early stage. An absorption type heat pump can also reach a high temperature to generate steam, but its performance is lower than that of the vapor compression type heat pump. Xue et al. [20, 21] produced steam using an absorption heat pump with zeolite-water and performed dynamic modeling of production rate. Liu et al. [22] applied a vertical heat exchanger to an absorption heat pump to produce steam. On the other hand, Qpinch [23] introduced a chemical heat transformer that raises the temperature from 75-125℃ to 110-190℃. This heat pump uses the principle that polymer absorb/release heat when it hydrolyze/dehydrate water.

Most of the research on the high-temperature heat pump is focused on vapor compression type. Vapor compression type heat pumps can generate more condensing heat from the same input energy source than a boiler. Park et al. [24] suggested that if the temperature difference from waste heat to discharge is significant, the heat pump can be sequentially arranged to obtain the maximum COP and required heat amount. Since the heat pump using R245fa requires a higher degree of superheat as the evaporating temperature is lowered, studies on cascade or sequential cycles are carried out.

Table 1.1 Refrigerants which have a critical point above 140℃

(a) Chemical refrigerants

		ODP	GWP	P_c (kPa)	T_c (℃)	Safety
R141b	HCFC	0.12	725	4250	204.2	A2
R365mfc	HFC	0	794	3266	186.85	B1
R123	HCFC	0.02	77	3662	183.68	B1
R21	HCFC	0.04	151	5180	178.45	B1
R245ca	HFC	0	693	3925	174.42	B1
R245fa	HFC	0	1030	3640	154.05	A1
R1234ze(Z)	HFC	0	6	3640	150.12	A2L

(b) Natural refrigerants

	ODP	GWP	P_c (kPa)	T_c (℃)	Safety
Water (R718)	0	0.2	22060	373.95	A1
Methyl formate (R611)	0	25	6000	213.55	B2
Pentane (R601)	0	4	3358	196.56	A3
Diethyl ether (R610)	0	4	3640	193.65	A3
Iso-Pentane (R601a)	0	4	3378	187.78	A3
Butane (R600)	0	4	3796	152.01	A3
Carbon Dioxide (R744)	0	1	7380	31.04	A1

To use a vapor compression type heat pump at an operating temperature higher than usual (making hot water), it is necessary to choose an appropriate refrigerant. The refrigerant should have a high critical point for two-phase heat exchange at the steam generation temperature. The refrigerants with non-flammability and non-toxicity complying with ASHRAE safety standards are preferred [25]. A/B means toxicity, 1/2/2L/3 means flammability. On this basis, Table 1.1 shows that R245fa is the optimum refrigerant meeting the conditions. Many artificial refrigerants have toxicity, and hydrocarbon refrigerants such as butane are flammable. In natural refrigerants, the carbon dioxide cycle has the disadvantage of controlling the supercritical cycle at high pressure. Recently, several HFO (Hydro-flurro-olefin) refrigerant with low GWP (global warming potential) were investigated [26]. Refrigerants such as R1234ze(Z), R1336mzz(Z), R600, R601, Carbon dioxide, and water have been studied. Carlos et al. [53] additionally suggested R1224yd(Z) for newly added environmental regulations.

Many refrigerants were compared to select the optimal refrigerant for the SGHP, before developing the specific components of the SGHP cycle. The primary criterion for selecting refrigerant is that two phases of heat transfer are possible at the steam temperature. Recent studies focused on choosing the optimal refrigerant through a single cycle analysis. For comparison of refrigerants, each condition (degree of superheat, degree of subcooled, and temperature lift) were kept constant. Kondou et al. [27] showed a high COP of

R1234ze(Z) and R365mfc at a condensation temperature of 160℃. Wang et al. [17] showed that R1233zd(E), R1234ze(Z), R245fa, and R600 (Butane) were suitable in the condensation temperature range above 100℃. The authors also simulated 13 low GWP refrigerants at diverse temperature ranges. As a result, R1234ze(Z) showed a relatively high COP above 100℃. Xiaohui et al. [28] operated a heat pump with a near-azeotropic refrigerant mixture named BY-4. The authors showed a heat pump cycle with a COP of 3.5 at a temperature of 110℃. Hydrocarbon, R1234 series, R245ca, and R365mfc, which have flammability and toxicity, are excluded from considering system safety. R11 is also excluded because it is CFC (Chlorofluorocarbon) refrigerant with a high ODP (Ozone depletion potential), and its use is gradually prohibited. Therefore, R245fa is the most suitable refrigerant for the temperature range of SGHP, and ORC (Organic Rankine cycle).

Additionally, Gupta et al. [29] calculated and compared the performance of low GWP HFO refrigerants. El-sayed et al. [30] organized the heat transfer properties and compatibility with lubricating oil beyond the ODP, GWP, toxicity, and flammability of the refrigerants. Wu et al. [31] simulated R1234ze(Z) and CO_2 hybrid heat pump system and conducted exergy analysis. Arpagaus et al. [32] summarized the heat demand of industries by temperature and heating capacity. The authors intensively reviewed six refrigerants (R1336mzz(Z), R718, R245fa, R1234ze(Z), R600, R601). Yu et al. [33] researched binary mixture refrigerant. A parameter estimation method was

developed to predict energy and exergy analysis. Fukuda et al. [34] experimented R1234ze(Z) (GWP=7) heat pump with twin rotary compressor and calculated ideal COP. Helminger et al. [35] experimented IHX cycle using a piston compressor, where the compression ratio of R1336mzz(Z) cycle is less than that of R245fa and R1234ze(Z). Nilsson et al. [36] also investigated the internal heat exchanger cycle with a piston compressor with this refrigerant and calculated ideal COP.

On the other hand, a high-temperature heat pump using natural refrigerants are researched. Typically, there are carbon dioxide and water. Heat pumps using CO_2 as refrigerant have been investigated. The critical temperature of CO_2 is 31.1℃, and a heat pump above 100℃ becomes a trans-critical cycle. White et al. [37] created an experimental device to make water above 65℃ with a CO_2 heat pump. Based on the experimental data, a computer simulation shows the expected data above 100℃. Opeyemi et al. [38] suggested through review articles that the compression technique of the CO_2 heat pump should be developed. Kim et al. [39] evaluated the results of the CO_2 heat pump with the ejector and internal heat exchanger. The authors show that the charge amount and mixing section diameter has an optimal value. Baik et al. [40] simulated optimal CO_2 heat pump cycle for the high-temperature range. There are also researches on a heat pump using water as a refrigerant. Chamoun et al. [41-42] have conducted a series of studies on dynamic modeling, an analysis based on Modelica on twin screw compressors, and analytical-experimental tests.

Madsboell et al. [43] and Larminat [44] studied the heat pump system using a centrifugal water vapor compressor. Shen [45] also examines water compressors. Bamigbetan et al. [46-47] theoretically evaluated the refrigerants. The results show that hydrocarbons and halocarbons are the most promising candidates. The authors also show cascade heat pump with propane and butane. The prototype butane compressor was investigated for the parameter study.

Studies on steam generation heat pumps can be summarized into temperature range and cycle configuration in addition to the refrigerant [32]. Studies of heat pump using the same R245fa refrigerant can be divided into different temperature range. Bobelin et al. [48] performed COP 2.5 at a temperature of 50 to 120℃ by using scroll compressors and an IHX. Wolf et al. [49] achieved COP 3.4 at a temperature of 50~100℃ using a piston compressor. Wilk et al. [50] showed COP 2.2 at a temperature of 50~120℃ and COP 2.3 at a temperature of 60~130℃ using a screw compressor and internal heat exchanger type vapor injection.

Heat pump systems with a piston (reciprocating) compressor and internal heat exchanger have been researched. Lee et al. [51] experimented with a 30 kW heat pump and achieved COP 3.5 at a temperature of 60~105℃, and Wang et al. [52] experimented with a 100 kW heat pump and achieved COP 3.05 at a temperature of 70~120℃. The variables that can improve the performance of the steam generation heat pump system were listed. Due to the characteristics of the R245fa, which must have a high degree of superheat, the introduction of

the injection cycle did not improve performance. The factors can be categorized by introducing the internal heat exchanger, insulating the system, and optimizing the steam pressure.

Carlos et al. [53] summarized recent studies as shown in Figure 1.8 according to the temperature range. The terms ‘high-temperature heat pump (HTHP)’, ‘very high-temperature heat pump (VHTHP)’ are used depending on the temperature of the heat sink and the heat source. Research has recently been conducted to produce condensing temperature above 100℃ using heat source temperatures below 100℃. The authors compared the refrigerants and system configurations with the internal heat exchanger and two-stage compression. The authors also suggested the future vision of the combining the heat pump and organic Rankine cycle. Steam generation heat pump technology can be expanded to a means of renewable energy storage thermally.

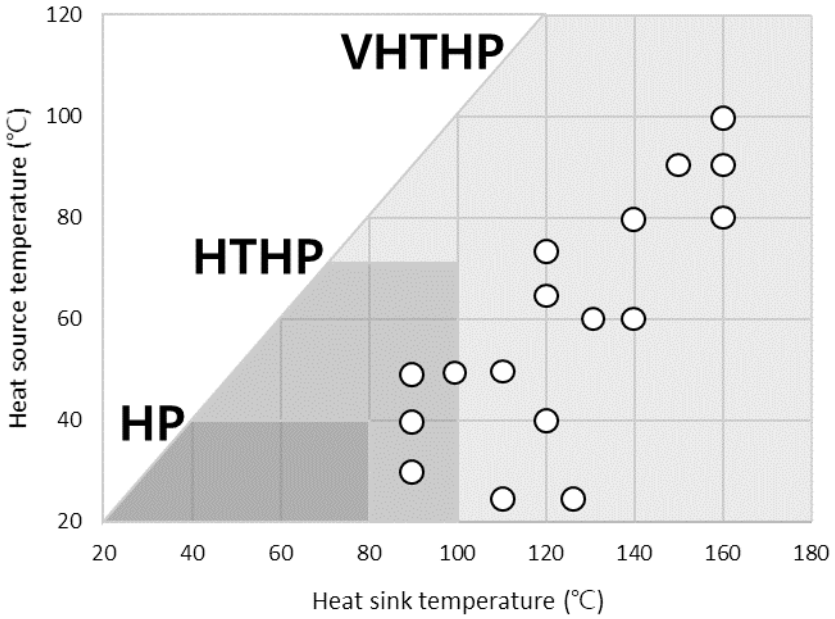

Fig. 1.8 Recent research cases of high-temperature heat pump

1.2.3 Water boiling and two-phase operation

The difference between the conventional heat pump and the steam generation heat pump is the condensing part. Water circulates between the reservoir and the heat exchanger to increase the amount of heat exchange. The brazed plate heat exchanger is usually used as a condenser of the heat pump, and the flash tank is usually used as a reservoir of two-phase water. Two-phase water and feed water are mixed and circulated through the condenser and flash tank. The generated steam is directly used or mechanically recompressed as required. Kang et al. [53] summarized the differences and similarities between the flash tank of steam generation heat pump and mechanical vapor recompression system. There is also a study focusing on components. Opeyemi et al. [38] reviewed the circulation of water vapor from a lower pressure to higher pressure using a compressor. The authors thought centrifugal compressor with a high flow rate and low-pressure ratio because of its low density are key factors.

As shown in Figure 1.9, a commercial steam generation heat pump system is shown, which is similar to the existing MVR. however, the results are quite different. As an output, MVR requires steam (B) or condensate (C) while the steam generation system requires steam (B) or re-pressurized steam (C'). This is because the purpose of the MVR is mostly distillation, and the use of the steam generation heat pump is to produce steam under certain conditions.

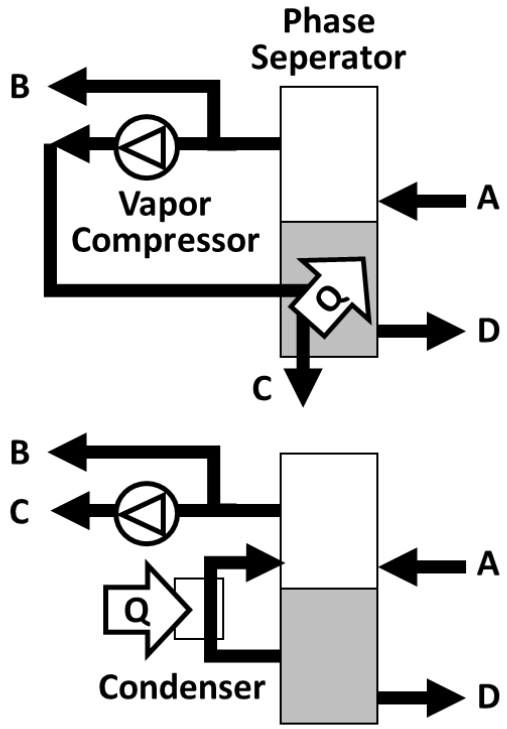

Input	A	Product to be evaporated
Output	B	Vapor
	C	Concentrated product
	C’	Recompressed vapor
Drain	D	Concentrated product

Fig. 1.9 Schematic diagram of MVR and SGHP

MVR is classified as an open heat pump, and an extension of the vapor compression heat pump technology. Its usage varies as follows. For desalination, reverse osmosis (RO) method is becoming popular, and MVR is not so popularly used today. Jogwar et al. [54] suggested a dynamic modeling and controller logic of vapor recompression distillation system, where the refrigerant is propane-propylene. Zhou et al. [55] showed that MVR is also able to apply to wastewater distillation. By experiment with laboratory prototype, the authors showed that the specific power consumption increased in proportion to the temperature difference. Onishi et al. [56] suggested new nonlinear model, and a case study supported it. As a result, it has been shown that MVR can be used for shale gas flow-back water treatment.

There are researches based on a pinch, energy, and exergy analysis of MVR. Han [57] suggested a single and double stage MVR. As a result, multi-stage is advantageous in terms of energy saving potential, and middle discharged mass concentration is a key variable. Walmsley et al. [58] suggested process flow and grid diagram. The authors pointed out that the 'Grand Composite Curve' shows the position of MVR that results in energy reduction. Kazemi et al. [59] simulated various configurations of the system. Based on energy, utility consumption, and costs, the best arrangement is chosen. Bless et al. [60] compared the energy-CO_2 emission-economic aspects of the two steam generation methods. Comparing the direct heating system, MVR was advantageous because it added waste heat recovery.

1.3 Objective and scopes

The heat pump has advantages in terms of energy for waste heat recovery and steam generation than conventional cooling tower and boiler. However, studies of heat pumps over 100℃ that can boil water are at an early stage. Besides, unlike hot water generation, the steam generation shows a change in temperature strictly depending on the pressure of the flash tank. To study the above behavior, numerical simulation, experimental study, and dynamic modeling were performed. A flash tank (phase separator) and a vapor compression type heat pump using R245fa as a refrigerant is used for the experiment.

In chapter 2, before the experiment, static modeling is presented to simulate the effect of the internal heat exchanger and its configuration change. The way for experiment with the configuration change of the internal heat exchanger was also sought.

In chapter 3, the relationship between key factors and the performance was investigated through experiments. The performance according to the temperature of the heat source and the flash tank was suggested. The heat capacity in the internal heat exchanger was controlled by bypass rate, and the effects were observed.

In chapter 4, the transient behavior of the combination of the heat pump and the flash tank at starting-up or transient-state condition is predicted and verified with the experimental data. The model is expressed in the form of time

domain transfer function. The start-up process was divided into several stages according to the temperature conditions of the heat source and the flash tank, and each stage shows different behavior.

In the last chapter, a brief summary of the study and conclusion are given.

Chapter 2. Analytic study on the high temperature heat pump with internal heat exchanger

2.1 Introduction

The saturated vapor line of R245fa shows a positive tendency. High DSH (degree of superheat) is required at the evaporator outlet to prevent liquid compression in the compressor. Lee [61] shows that it is necessary to secure a DSH for each combination of the heat source and heat sink temperature for safe compression. At a condensing temperature of 125℃, DSH required 15, 12, and 10℃ when the evaporating temperature is 60, 70 and 80℃. Figure 2.1 shows an example of single R245fa heat pump cycle. Large DSH reduces the overall performance of the system. Therefore, the cycle change to lower DSH is considered. The introduction of the internal heat exchanger (IHX) is expected to lower the DSH, the compression work, and the compressor discharge temperature.

In this chapter, the numerical simulation of heat pump cycle with internal heat exchanger was conducted in various conditions. Before the simulation of the transient behavior of steam generation with the pressurized flash tank was conducted, the numerical analysis of heat pump cycle should be validated for the comparison of performance.

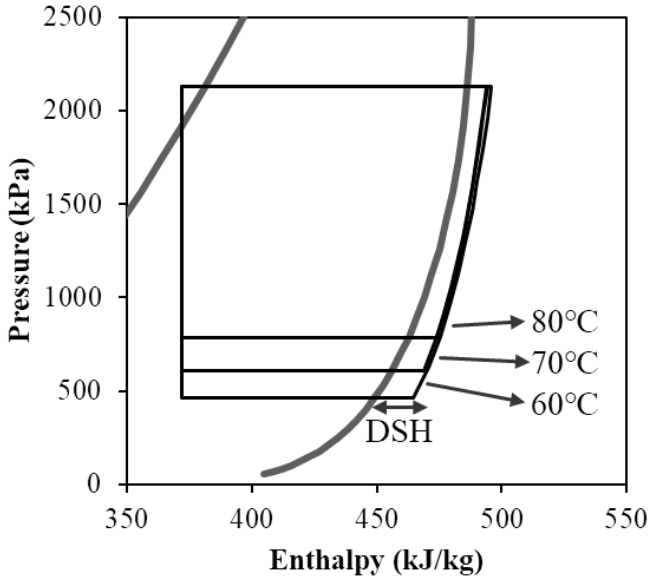

Fig. 2.1 Pressure-enthalpy diagram of R245fa heat pump cycle with various evaporating temperature

2.2 Components modeling

2.2.1 Compressor

The compressor in the heat pump determines the compressor work, the pressure ratio and mass flow rate of refrigerant. In this study, the type of compressor was selected as as reciprocating type compressor as same as the experiments. The steady state modeling of compressor was designed that if the input data, condensing pressure, evaporating pressure and compressor speed was determined, the output data could be obtained. The compression process is assumed to be a polytropic process. The polytropic number of the compression process is obtained as shown in Equation (2.1) and Figure 2.2. The average polytropic number obtained using the existing experimental data was 0.987.

$$n_{poly} = \log\left(\frac{P_{out}}{P_{in}}\right) / \log\left(\frac{\rho_{out}}{\rho_{in}}\right) \quad (2.1)$$

The mass flow rate of the compressor was obtained by multiplying the stroke volume, the inlet density of the refrigerant, the rotational speed, and the volumetric efficiency. Volumetric efficiency was obtained from the gap volume ratio, the compression ratio, and the polytropic coefficient. The smaller the polytropic coefficient, the lower the volumetric efficiency, mass flow rate and compression work.

$$\dot{m} = V\rho_{in}v\eta_V \tag{2.2}$$

$$\eta_V = 1 - C\left(\left(\frac{P_{out}}{P_{in}}\right)^{\frac{1}{n_{poly}}} - 1\right) \tag{2.3}$$

The thermodynamic properties of the refrigerant at the outlet of the compressor were calculated as Equation (2.4). The average polytropic value from the Equation (2.1) and the properties at the inlet of the compressor were used. The compression work was calculated based on the product of mass flow rate of the refrigerant and the enthalpy of the inlet and the outlet of the compressor.

$$\rho_{\mathrm{out}} = \rho_{\mathrm{in}} \times \left(\frac{P_{out}}{P_{in}}\right)^{\frac{1}{n_{poly}}} \tag{2.4}$$

Compression efficiency is obtained as shown in Equation (2.5) and Figure 2.3. Compression efficiency decreased with degree of superheating (DSH, Temperature difference between compressor inlet and gas saturation temperature).

$$\eta_{mech} = \mathrm{W_{cal}}/W_{real} \tag{2.5}$$

The results of compressor modeling for estimating the mass flow rate of the refrigerant and compression work is shown in Figure 2.4. The mass flow

rate of the refrigerant and compression work fit well within the 5% margin of error. The compressor modeling was used for the analytic studies of the single cycle, the internal heat exchanger cycle, and transient modeling.

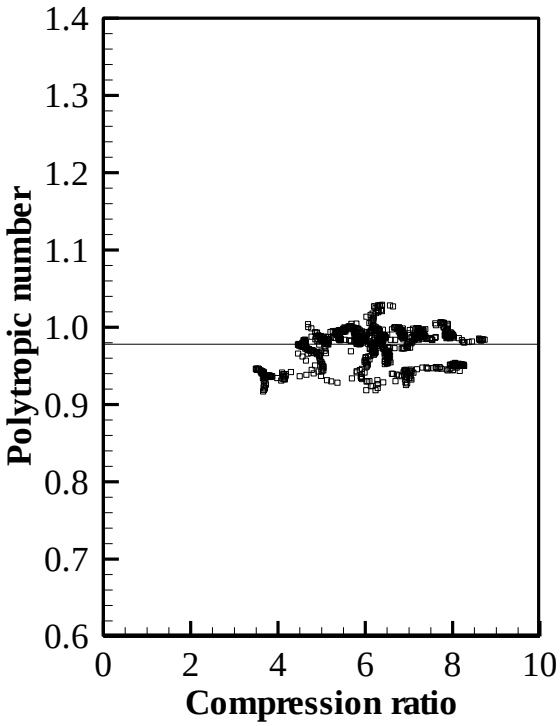

Fig. 2.2 Polytropic number of the compressor

by the compression ratio

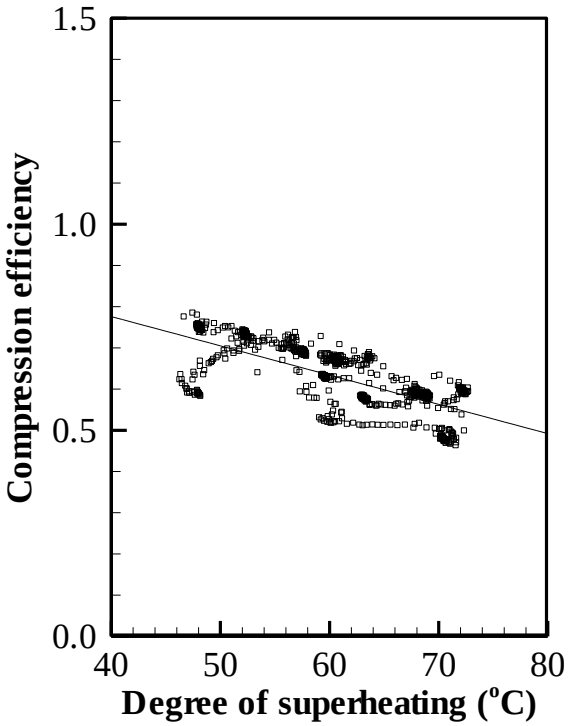

Fig. 2.3 Compression efficiency of the compressor

by the degree of superheating

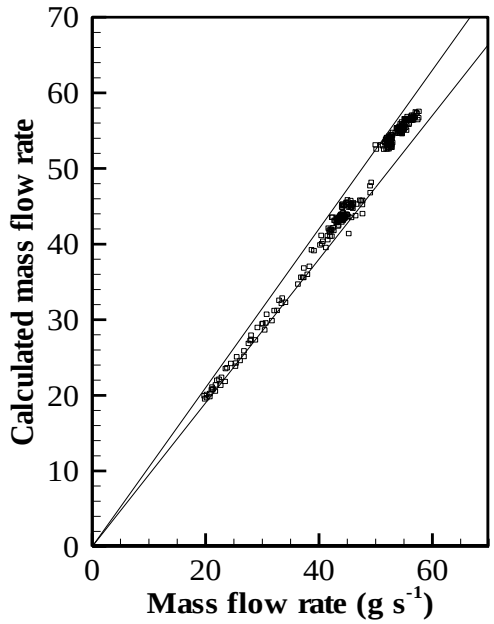

(a) Mass flow rate

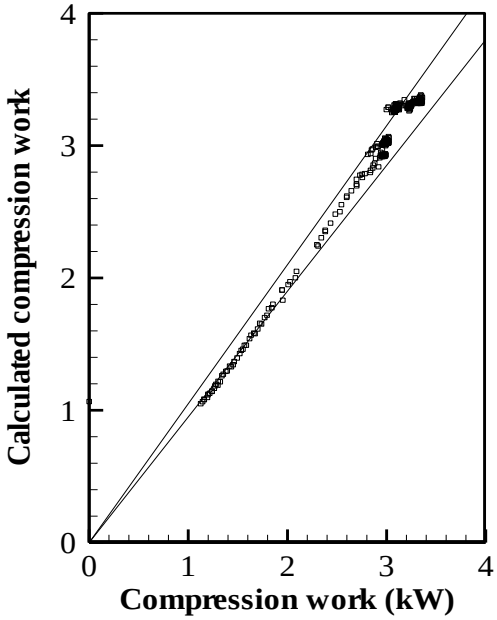

(b) Compression work

Fig. 2.4 Comparison of experimental data and calculated values

2.2.2 Heat exchanger

The counterflow plate heat exchangers were used in the experiments. The heat exchangers are assumed to me one-dimensional counterflow heat exchangers. Heat transfer amount can be obtained by multiplying mass flow and enthalpy difference. It is assumed that there is no heat loss and pressure loss in the heat exchanging process.

The heat transfer coefficient depends on the phase and the condition (condensing, evaporating) of the fluid. The heat transfer coefficient of the plate heat exchanger of Yan et al. [62-63] was used. The analysis was carried out by changing the refrigerant because of the formulas used in typical plate heat exchangers. The heat transfer coefficients used in the modeling are given in Table 2.1.

The epsilon-NTU method was used. The heat exchanger is divided into n grids, where the result of the heat exchange of two fluids (R-245fa, Water) in the i-th grid is reflected in the (i+1)-th grid. The properties of the refrigerant inlet and the water inlet is already given. The iteration can be finished if the input value of the second fluid matches the known value. If not, change the input value of the first grid and start a new calculation. The calculated result is reused as an assumed value to converge. The process of convergence is shown in Figure 2.5.

Table 2.1 Heat transfer coefficients used in modeling

Fluid	Condition	(Local) Heat transfer coefficient
Refrigerant	Two phases Condensing	$ec = (1 - x + x\left(\frac{\rho_l}{\rho_v}\right)^{0.5})$ $G_{eqv} = \frac{\dot{m}ec}{A_{path}}$ $\mathrm{Re_{eqv}} = \frac{G_{eqv}D_h}{\mu}$ $\mathrm{Nu} = 4.118\mathrm{Re_{eqv}^{0.4}Pr^{1/3}}$ $\mathrm{htc} = \frac{\mathrm{Nuk}}{\mathrm{D_h}}$
	Two phases Evaporating	$\mathrm{Bo} = \frac{\mathrm{Q_{wall}}}{G_{eqv}(h_v - h_l)}$ $\mathrm{Nu} = 1.926\mathrm{Re_{eqv}^{0.5}}Pr^{1/3}\mathrm{Bo^{0.3}}ec$ $\mathrm{htc} = \frac{\mathrm{Nuk}}{\mathrm{D_h}}$
	One phase	$\mathrm{Nu} = 0.2121\mathrm{Re^{0.78}Pr^{1/3}}$ $\mathrm{htc} = \frac{\mathrm{Nuk}}{\mathrm{D_h}}$
Water	One phase	$\mathrm{Nu} = 0.2121\mathrm{Re^{0.78}Pr^{1/3}}$ $\mathrm{htc} = \frac{\mathrm{Nuk}}{\mathrm{D_h}}$

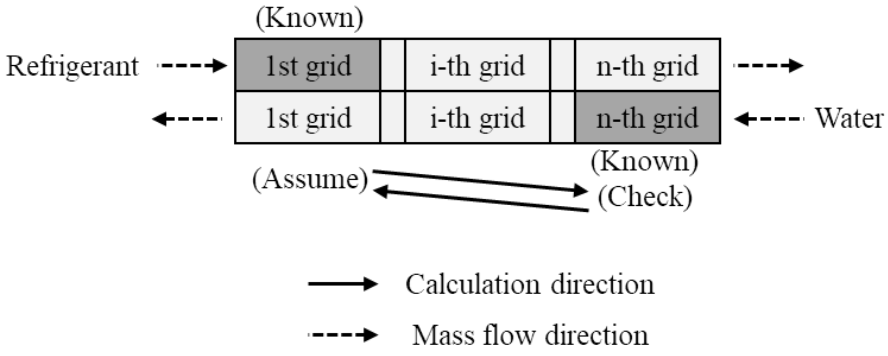

(a) One-dimensional counterflow heat exchanger

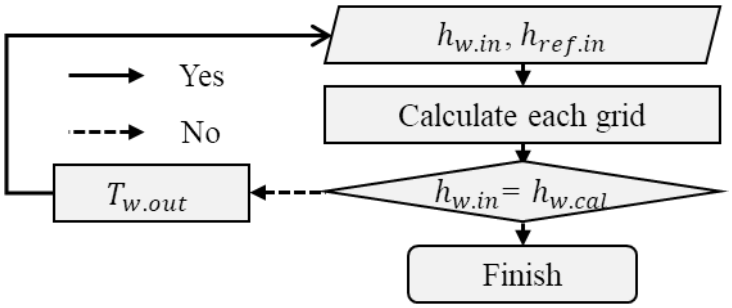

(b) Flow Chart

Fig. 2.5 Calculation process of the heat exchanger

2.2.3 Flash tank

Like the accumulator, the quality was confirmed according to the enthalpy of the flash tank. The calculation was different depending on the before and after the target temperature. Prior to the target temperature, it is assumed that the condensing heat was used to pressurize tank without the inlet and the outlet flow.

$$\dot{m}_{steam} = \dot{m}_{feed} = 0 \tag{2.6}$$

$$\Delta h = \frac{\dot{m}_{circ}(h_{FT.in} - h_{FT.out})}{M_{FT}} \tag{2.7}$$

After the flash tank reaches its target temperature, it was assumed that the condensing heat was equal to the steam outlet. In addition, it is assumed that water is supplied as much as the steam outlet. In this case, the steam generation rate is the condensing heat divided by the difference of two enthalpy.

$$\dot{m}_{steam} = \dot{m}_{feed} = \frac{Q_{condenser}}{h_{steam} - h_{feed}} \tag{2.8}$$

$$\Delta h = \frac{\dot{m}_{circ}(h_{FT.in} - h_{FT.out}) + \dot{m}_{steam}(h_{feed} - h_{steam})}{M_{FT}} \tag{2.9}$$

2.3 Cycle modeling

Before modeling the internal heat exchanger cycle, the single (or simple) cycle is analyzed. Single heat pump cycle means a cycle consisting of only the compressor, expansion valve, and heat exchangers (condenser, evaporator). The expansion process assumes that the enthalpy of the condenser outlet is the same as the enthalpy of the evaporator inlet.

The condensing pressure was determined depending on whether the evaporator outlet enthalpy coincided with the compressor inlet enthalpy. The evaporating pressure was determined depending on whether the calculated refrigerant charge amount coincided with the target refrigerant charge amount. The median of the upper and lower boundaries is substituted into the new boundary.

The charge amount of the refrigerant was assumed to be a refrigerant filled between two pipes connecting the condenser and the evaporator. The refrigerant charge amount of the pipe from the evaporator outlet to condenser inlet was calculated by the density at the inlet of the condenser. The refrigerant charge amount of the pipe from the condenser outlet to evaporator inlet was calculated by the density at the outlet of the condenser.

Unlike the heat pump cycle using the shell and tube heat exchanger, the heat pump cycle using the plate heat exchanger has a small amount of refrigerant in the heat exchanger. The amount of liquid state refrigerant in the pipe influences the total charge amount of refrigerant in the cycle.

Figure 2.6 shows the flow chart of internal heat exchanger cycle calculation. The internal heat exchanger cycle exchange heat between the refrigerant after the condenser and the refrigerant after the evaporator. Except for the internal heat exchanger calculation in the flow chart, it is same as the calculation of single cycle. The internal heat exchanger allows a simultaneous increase of condensation heat and evaporation heat, but degree of superheating, discharge temperature of the compressor, and compression work can be increased. Incidentally, the evaporation pressure may converge depending on DSH, and the condensing pressure may converge depending on charge amount.

For the calculation of the internal heat exchanger, the property of the evaporator outlet, which is the inlet of the lower part of internal heat exchanger, is assumed. The inlet and outlet temperature of the internal heat exchanger cannot be lower than the evaporator outlet temperature or higher than the condenser outlet temperature. Iteration proceeds so that the enthalpy exchange amount of the higher temperature part and the lower temperature part of the internal heat exchanger are the same.

After the components are calculated, the condensing pressure and the evaporating pressure are determined. Most (70~80%) of the refrigerant charge amount is in the liquid pipe and higher temperature part of the internal heat exchanger. Shortening the length of the liquid line can reduce the amount of refrigerant usage.

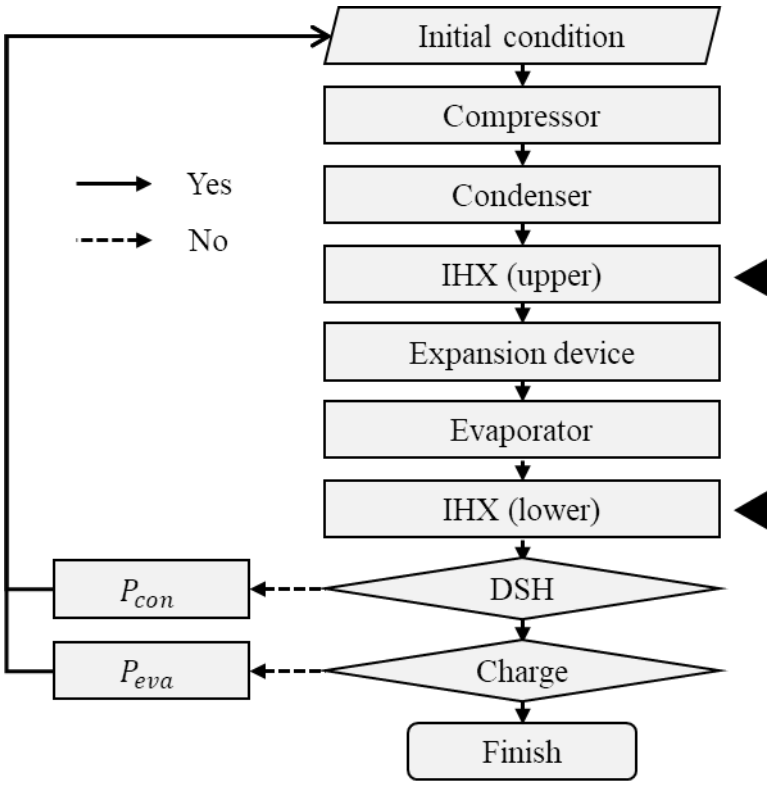

Fig. 2.6 Flow chart of internal heat exchanger cycle calculation

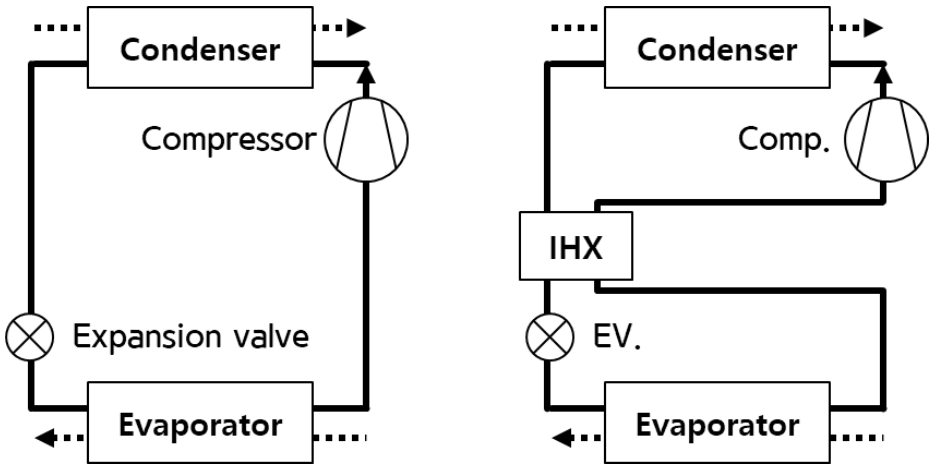

(a) System configuration

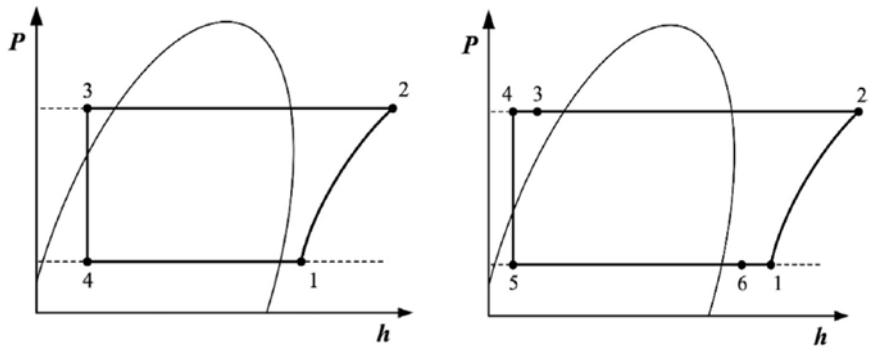

(b) Pressure-enthalpy diagram

Fig. 2.7 Schematic diagram of single and internal heat exchanger cycle

2.4 Results and discussions

Figure 2.8 shows the COP based on system configuration and temperature range. The heat source range was between 40℃ (which waste heat can be discharged to the river) and 80℃ (which is useful in the industrial field). The higher the heat source temperature and the lower the flash tank temperature, the lower the compression ratio and the higher the COP. When the heat sink temperature changed, the internal heat exchanger cycle always had 16 to 30% higher COP than the single cycle.

Experimental data were limited to those with positive DSC and DSH. Unlike the results of the modeling, two-phase refrigerant was discharged from the outlet of the condenser when the heat source temperature is high. In this case, the enthalpy could not be specified only by measuring temperature and pressure at the outlet of the condenser. In addition, to increase the saturation temperature of the water in the flash tank, the pressure should be increased greatly, so it was only tested up to 125℃ for safety.

Modeling and experimental results were well-fitted as shown in the figures. The change of the condensing heat more attributed the change in COP more than compression work. The change of mass flow rate of refrigerant of the internal heat exchanger cycle was smaller than that of single cycle.

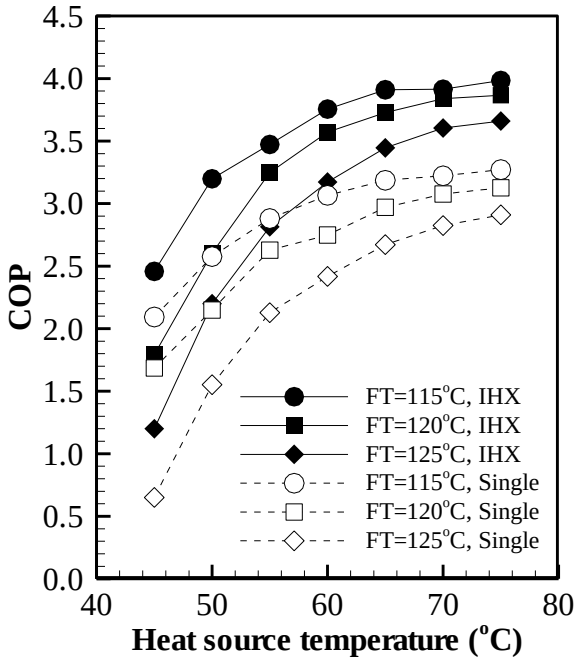

(a) COP per heat source temperature (T_{FT}=120℃)

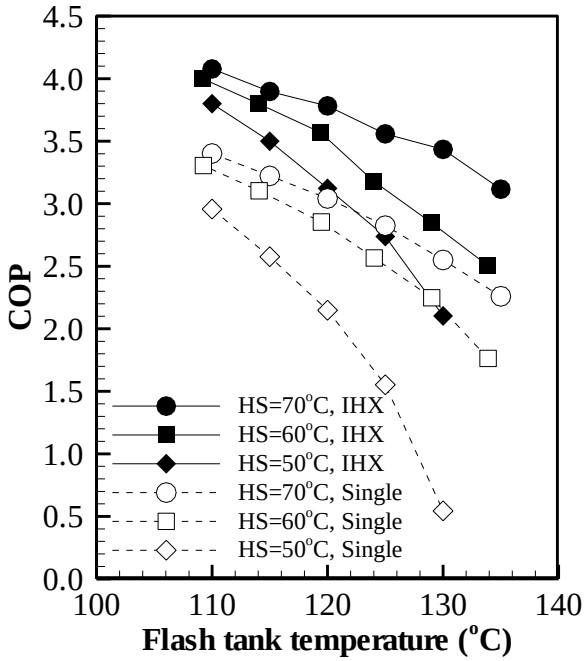

(b) COP per flash tank temperature (T_{HS}=60℃)

Fig. 2.8 Change of the COP by the system configuration

As shown in Figure 2.9, the temperature at inlet and outlet of the internal heat exchanger was observed. The outlet temperature of the lower side of the internal heat exchanger is close to the inlet temperature of the higher side of the internal heat exchanger. It means that the compressor inlet temperature of the internal heat exchanger cycle will be the condenser outlet temperature. In addition, it means that the heat exchange amount depends on the heat source temperature and the heat sink temperature.

The previous modeling and experimental data used an internal heat exchanger whose effectiveness (ε) was close to 1. The effectiveness of the heat exchanger is given in Equation (2.10). If the size of the heat exchanger is not sufficient, the performance is degraded. To verify the performance of the various size of the internal heat exchanger, the concept of mass flow split ratio is introduced. It means the ratio of input to the internal heat exchanger when a part of the refrigerant is diverted by bypassing the refrigerant at the outlet of the evaporator as shown in Equation (2.11).

$$\varepsilon = \frac{Q_{real}}{C\_\min \times \triangle T} \tag{2.10}$$

$$\text{Mass flow split ratio} = \dot{m}_{ihx} \div \dot{m}_{cycle} \tag{2.11}$$

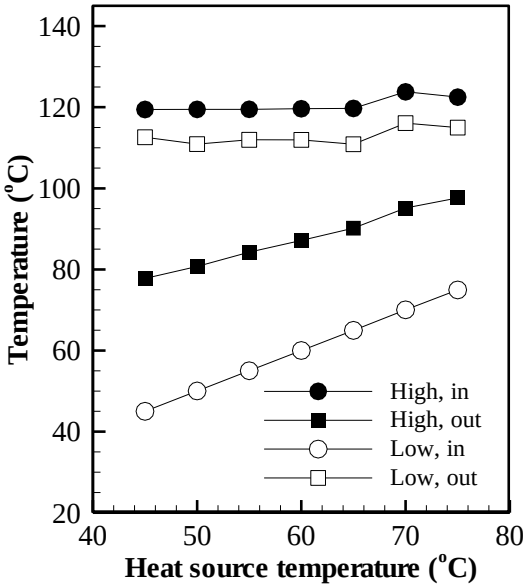

(a) Change by heat source temperature (T_{FT}=120℃)

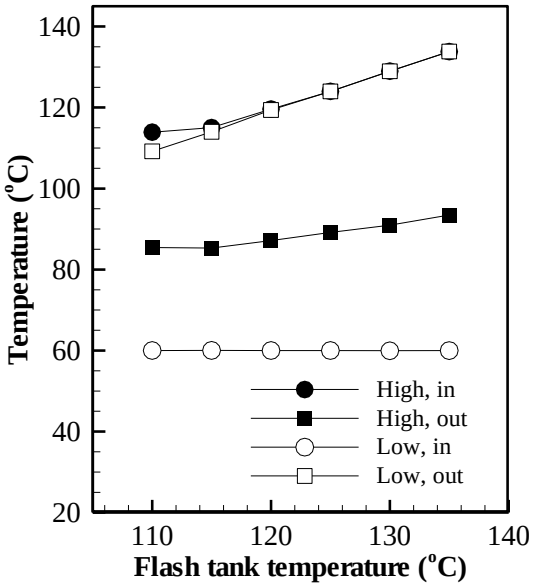

(b) Change by flash tank temperature (T_{HS}=60℃)

Fig. 2.9 The temperature of the inlet and outlet of the internal heat exchanger

Figure 2.10 shows the performance according to the size of the internal heat exchanger. The modeling results showed that the effectiveness and mass flow split ratio were similar. On x-axis, 0 means the single cycle and 1 means the internal heat exchanger cycle.

The experimental results were consistent with modeling until the mass flow ratio was 0.6, but then converged to specific COP. This is because in the preliminary experimental cases, the degree of supercooling after the condenser was not secured, and the two-phase refrigerant was discharged from the condenser. As a result, the condensing heat was measured and calculated in the same value.

The changes in the COP, heating capacity, compression work and pressure-enthalpy diagrams according to the effectiveness of the internal heat exchanger are discussed in detail in the next chapter.

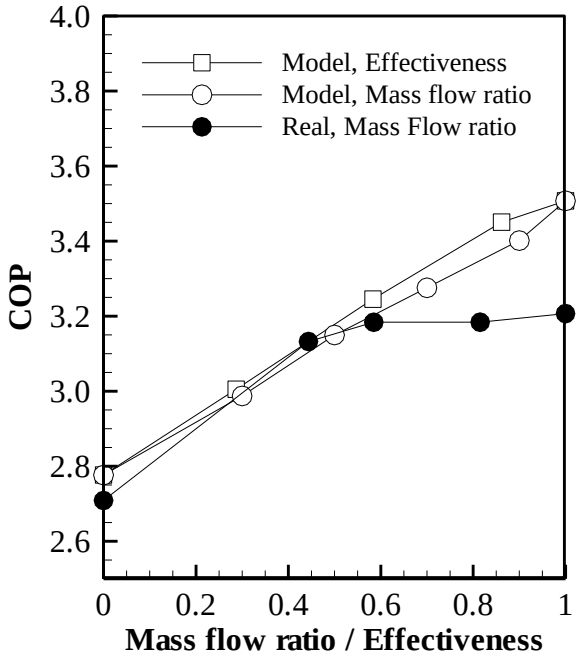

Fig. 2.10 Performance by the size of the internal heat exchanger

(T_{HS}=60℃, T_{FT}=120℃)

2.5 Summary

In this chapter, the performance of heat pump cycle with and without the internal heat exchanger were compared. Before the experiment chapter, the performance variation and operating method were verified by preliminary experimental data. The numerical analysis was carried out by components. The steady-state modeling converges the values after calculating the overall cycle modeling. Each process was simplified by assumptions and the complexity was reduced. The condensing and evaporating pressure of the heat pump cycle were converged by iterating calculation.

By the comparison of modeling and experiment, it was validated that the result of modeling was well matched with result of experiment. The experimental value was less than the model value due to heat loss. The error rate of the COP was about and 4.7%.

From the results of simulation, the effectiveness of the internal heat exchanger was shown to be controlled by mass split ratio as well as changing the size. The performance of the system can be changed by mass split ratio. Using this method, further experimental research is proceeded at the next chapter.

Chapter 3. Experimental study on the performance with the internal heat exchanging effect

3.1 Introduction

As stated in the previous chapter, the numerical investigation showed that the introduction of the internal heat exchanger would increase the heat pump cycle performance and heat exchange amount.

Selecting the appropriate size (effectiveness) of IHX for the experiment become a new problem to solve. The previous study for optimal sizing of the system is as follows. Santa et al. [63] produced a mathematical model of a steady-state water heat pump. Heat exchangers were described by differential equations so its optimal size can be suggested. Hervas-Balsco et al. [64] presented a model to find the optimal size (capacity) of a heat pump system based on low heat sources.

In this study, a heat pump system is investigated to improve system performance by using an internal heat exchanger. The IHX capacity was changed by controlling the mass flow split ratio with a bypass line around the IHX. The mass flow rate of water, refrigerant, and mass flow split ratio were changed, and the system performance was investigated.

3.2 Experimental setup

3.2.1 Experimental apparatus

The diagram of the steam generation heat pump system is shown in Figure 3.1, and Table 3.1 describes the specifications of each component in the lab-scale experimental setup. The vapor compression type is selected, and it consists of a reciprocating compressor, brazed plate heat exchangers (evaporator, condenser and internal heat exchanger), electric expansion valve, and centrifugal water pumps. In general cases, the size of the evaporator is designed to be smaller than that of the condenser, but the bigger evaporator is chosen to obtain sufficient waste heat recovery. Sufficiently large internal heat exchanger is selected since the bypass line is to be installed. Figure 3.2 shows a picture of a specific device.

R245fa is chosen as a refrigerant as stated in the introduction. Oh et al. [65] showed that there are no problems in operation over 100℃ for over 1000 hours. The two water pumps were installed to circulate the secondary fluid (i.e., water) from the reservoir to the evaporator, and from the flash tank to the condenser respectively. The feed water nozzle is located on the pipe between the pump inlet and outlet of the flash tank. The mass flow rate and water head were controlled by adjusting the water pumps. This helps reduce the probability of the water hammering at the water pump. The evaporating heat transfer rate was limited to the capacity of the electric heaters at the reservoir.

As shown in Figures 3.1 and 3.3, the refrigerant passed through the internal heat exchanger (C), and the bypass line (A) mixed after the internal heat exchanger (B). However, the bypass line is only on the low temperature side of the IHX, and all refrigerant passes through the IHX on the high temperature side of the IHX. Therefore, the low-temperature side has three points of HX end (A), mixed point (B), and IHX end (C), but the high-temperature side only has one point. However, by energy balance, the enthalpy of the high-temperature side is determined by the enthalpy depending on the mixing ratio on the low-temperature side. Unlike previous studies exchanging IHX of different sizes, this study confirmed a continuous change by experimenting with various mass flow split ratio.

Table 3.1 Specification of the system

Part	Specifications
Compressor	Semi-hermetic reciprocating compressor, four cylinders 7.5 Horse power, 3 Phase 380 V, 30 Hz
Heat exchanger (condenser, evaporator)	Brazed plate heat exchanger, herringbone corrugation type Width 124 mm, length 512 mm, 26 plates
Heat exchanger (internal heat exchanger)	Brazed plate heat exchanger, herringbone corrugation type Width 119 mm, length 289 mm, 40 plates
Water pump (condenser)	Inline type vertical multi-stage centrifugal pump
Water pump (evaporator)	Horizontal multi-stage centrifugal pump
Electric heater	Scoop type, 15 kW
Electronic expansion valve	Unipolar type, RS-485 Communication

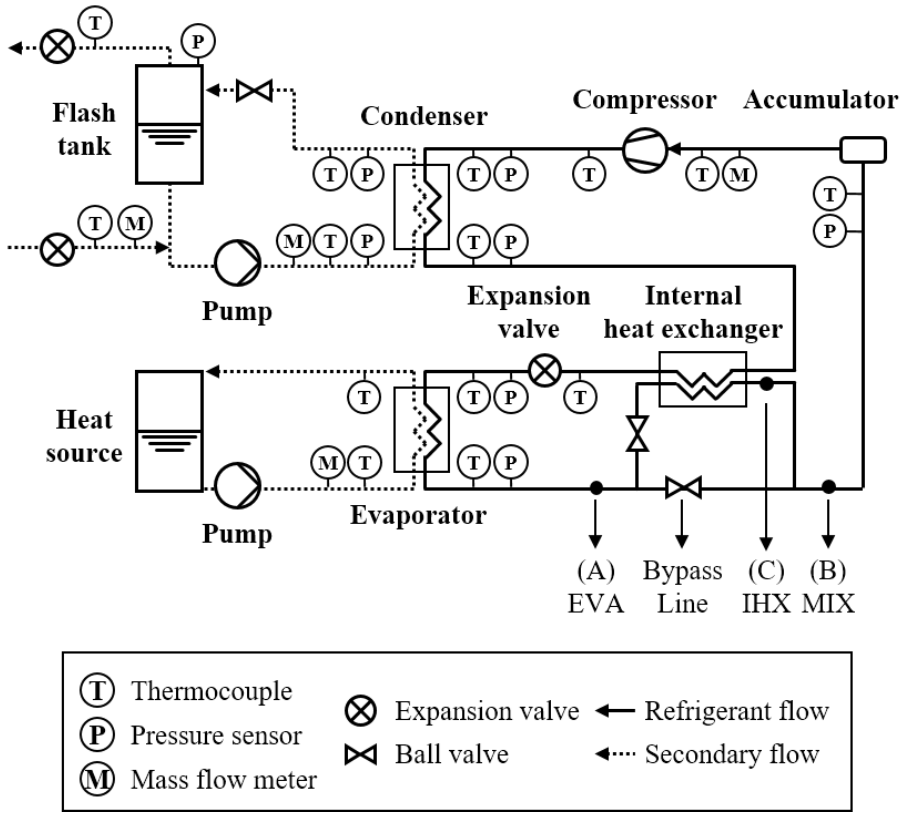

Fig. 3.1 Schematic diagram of experimental setup

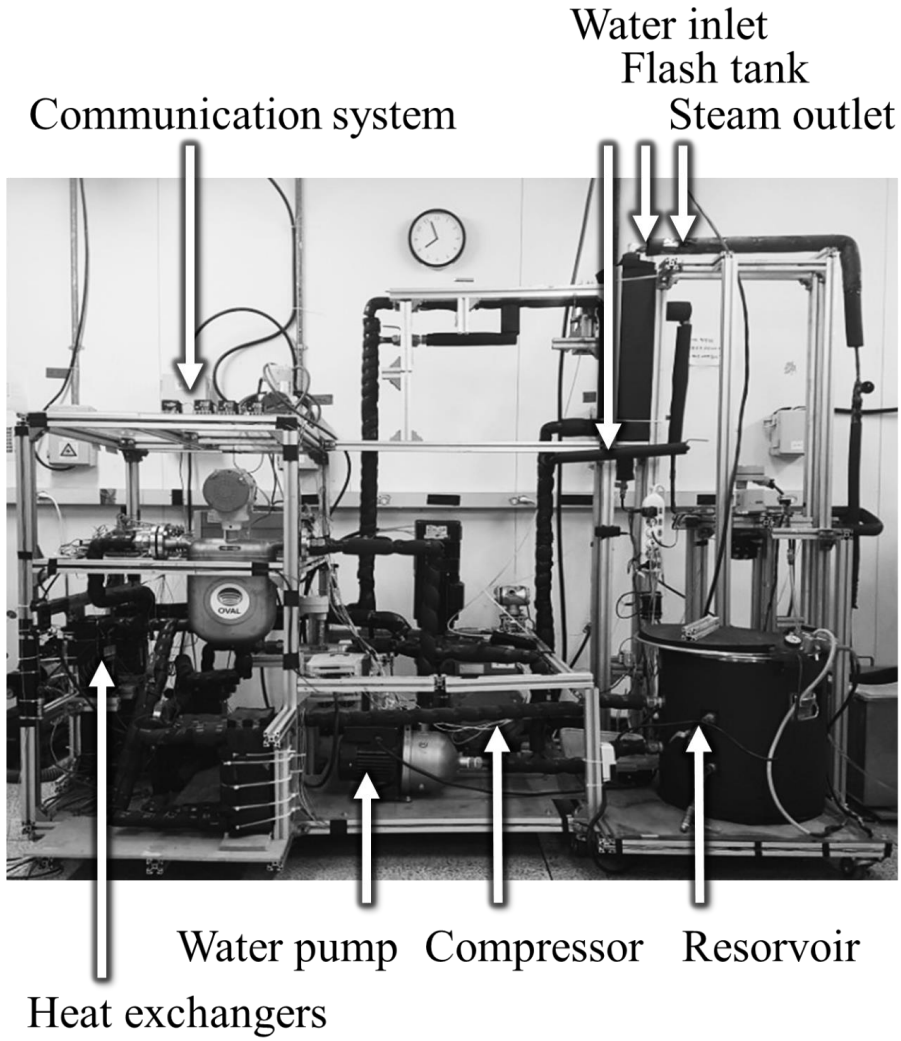

Fig 3.2 Configuration of experimental apparatus

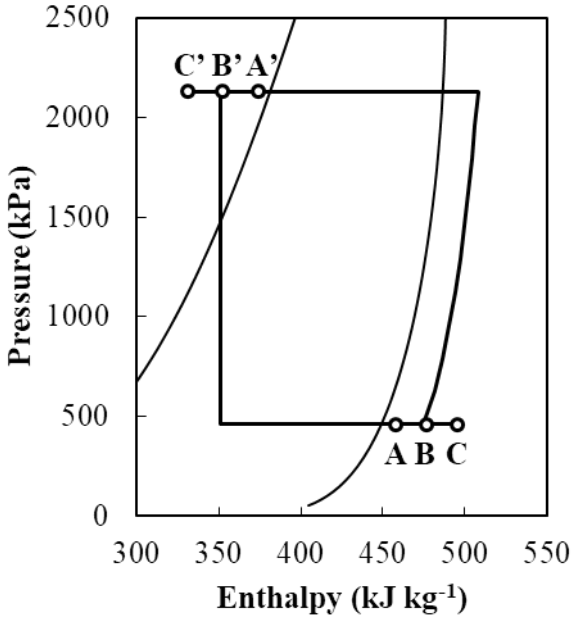

(a) Pressure-enthalpy diagram

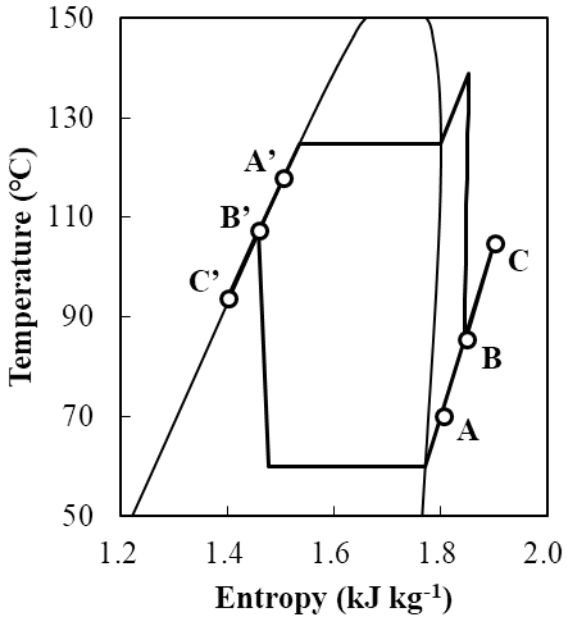

(b) Temperature-entropy diagram

Fig 3.3 Diagram of heat pump cycle with IHX

3.2.2 Uncertainty analysis and data reduction

The pressure transmitter at the branch of the pipe, Coriolis-type mass flow meter, and T-type thermocouple wire were used. The thermocouples were calibrated. Data were measured by every five seconds, and each experiment maintained a steady-state. Enthalpy was calculated from REFPROP 10.0 [66] from measured temperature and pressure. The heat transfer amounts of the heat exchangers are calculated by multiplying the enthalpy difference at the inlet and outlet by the mass flow rate of the refrigerant, as shown in equations (3.1) and (3.2). The heat of the generated steam is calculated by the difference between the enthalpy of water inlet and steam outlet of the flash tank, as shown in Eq. (3.3). It is assumed that the water inlet and steam outlet mass flow rate are equal if the water level at the flash tank is constant. The change in water level at the flash tank was measured by using a differential pressure gauge and sight-glass. The differential pressure gauge measures the pressure of the top and the bottom of the flash tank.

The compression work is measured by an input electric power meter. The COP of the system is obtained by dividing the condensate heat transfer rate by the compression work, as shown in Equations (3.4) and (3.5). The two COPs are equal due to the energy balance, but the COP of the refrigerant (3.4) is indicated in this study because its accuracy is higher than (3.5). The power consumption of the water pumps was ignored, because they correspond to less than 1% of the compression work of the heat pump.

$$\dot{Q}_{eva.ref} = \dot{m}_{ref} \times (h_{eva.ref.in} - h_{eva.ref.out}) \quad (3.1)$$

$$\dot{Q}_{con.ref} = \dot{m}_{ref} \times (h_{con.ref.in} - h_{con.ref.out}) \quad (3.2)$$

$$\dot{Q}_{steam} = \dot{m}_{steam} \times (h_{FT.steam.out} - h_{FT.water.in}) \quad (3.3)$$

$$\text{COP} = \dot{Q}_{con.ref} \div \text{W} \quad (3.4)$$

$$\text{COP}_{steam} = \dot{Q}_{steam} \div \text{W} \quad (3.5)$$

The uncertainty of the measured and derived data of the experiment is shown in Table 3.3 for the case with the best COP at a heat source temperature of 70℃. According to ASHRAE Guideline 2 [67], the propagation of error calculation is applied to derived values such as COP and heating transfer rate, respectively [68]. Maximum possible errors on the 95% confidence levels of the derived values are also presented in the table. The temperature was measured at 22 points, as shown in Figure 3.1, and the average of the error was written.

Table 3.2 Specifications of measurement instruments

Measured properties	**Specifications**
Pressure	Pressure transmitters (~10 bar)
Differential pressure	Differential pressure transmitter (~2 bar)
Temperature	T-type Thermocouple wires (-270~370℃)
Mass flow rate	Coriolis type mass flow meters (~100 g/s)
Power	Digital power meter (~600 V, ~20 A)

Table 3.3 Uncertainty analysis

Part	Overall uncertainty
Pressure (refrigerant, condenser inlet)	0.5%
Pressure (refrigerant, condenser outlet)	1.7%
Pressure (refrigerant, evaporator inlet)	1.5%
Pressure (refrigerant, evaporator outlet)	1.5%
Pressure (water, flash tank)	0.5%
Temperature (thermocouple, 22 points)	0.5℃
Mass flow rate (water, condenser)	1%
Mass flow rate (water, evaporator)	1%
Mass flow rate (water, feed water)	2%
Mass flow rate (refrigerant)	2%
Water level (water, flash tank)	0.1%
Compression work (electric power meter)	0.1%
Heating capacity (steam generation)	2.1%
Heating capacity (refrigerant, condenser)	2.6%
COP (steam generation)	2.1%
COP (refrigerant, condenser)	2.6%

3.2.3 Experimental conditions

The experimental conditions are shown in Table 3.4, and the experiments are carried out by changing the flow rates of the refrigerant and water. The refrigerant was charged to the design condition of 2.7 kg, which is the optimum charge amount for the lab-scale system known by conducting preliminary experiments.

The temperature condition of the heat source was diversified to 40 to 70℃ in order to simulate the performance of the heat pump according to the waste heat conditions. (Hot water above 80℃ is useful, is not called waste heat) Further, the temperature of the flash tank and the generated steam was set between 115 to 125℃.

The mass flow rate condition of the water in the condenser was varied from 400 to 800 g s^{-1}, and the water mass flow rate to the evaporator was varied from 300 to 1100 g s^{-1}. The speed of the compressor was fixed, and the refrigerant mass flow rate was changed by adjusting the opening ratio of electric expansion valve. The opening degree of the expansion valve was changed based on the evaporation temperature of the heat pump cycle instead of the mass flow rate of the refrigerant.

Table 3.4 Experimental conditions

Parameter	Value
Refrigerant charge amount (kg)	2.7
Heat source temperature (℃)	40 ~ 70
Flash tank temperature (℃)	115 ~ 125
Internal heat exchanger mass flow ratio (%)	0 ~ 100
Refrigerant mass flow rate (g s^{-1})	25 ~ 75
Condensing water mass flow rate (g s^{-1})	400 ~ 800
Evaporating water mass flow rate (g s^{-1})	300 ~ 1100

3.3 Results and discussion

3.3.1 The mass flow rate of the water in condenser

The system characteristics, such as COP (3.24), heat transfer rate at the condenser and evaporator (11.88, 8.12 kW), compressor work (3.67 kW), and steam generation rate (2.6 g s^{-1}), were shown to be less relative to the water mass flow rate of the condenser. The mass flow rate was variated by control the water pump rotating speed, but the condensing pressure and enthalpy were slightly changed, which is within the error range of the measurement. The condensing pressure, condensing saturation temperature, and compression discharge temperature decreased as the condensing water mass flow rate increased. In addition, as the water mass flow rate increased, the temperature difference between water and refrigerant was reduced.

However, when the pump power is lowered, the water mass flow rate is reduced, and the amount of pressure rise of the water is also decreased. If the water pressure is insufficient in the pipe connecting the condenser and the flash tank, water becomes two phases, and the mass flow rate fluctuates. The water pressure in the condenser could be sufficiently increased while lowering the water mass flow rate by the installation of the valve between the condenser and the flash tank.

Figure 3.4 shows the pressure-enthalpy diagram of the water circulating between the condenser and the flash tank. The amount of heat in the condenser

was fixed by adjusting the heat pump, and the mass flow rate of the water was fixed by controlling the pump. The dotted line is the saturated liquid line of water, and the area below the line means two phases. Points A to E indicates the process from when the water leaves the flash tank to return, as shown in Figure 3.5. The water in the flash tank comes out in a saturated liquid state and mixed with feed water. The pump pressurized the water. The enthalpy increases through the condenser, and the pressure drops. The water decompressed through the valve, and it returns to the flash tank. In this way, the introduction of the valve can determine the state of the water in the condenser outlet as the liquid (Case 1-2), and prevent water fluctuation.

The conventional heat pumps reduced the pressure drop of water in the condenser by setting the mass flow rate of water to 10 times higher than the refrigerant mass flow rate [7]. The mass flow rate of the water could be reduced from 10 to 3.5 times the mass flow rate of the refrigerant by the valve installation in this research. The flash tank is installed high to avoid cavitation in the pump. The mass flow rate of the pump can be safely reduced until the pressure of the condenser outlet satisfies the head of the fluid to the height of the flash tank. In other words, the mounting of the valve could lower the pump power.

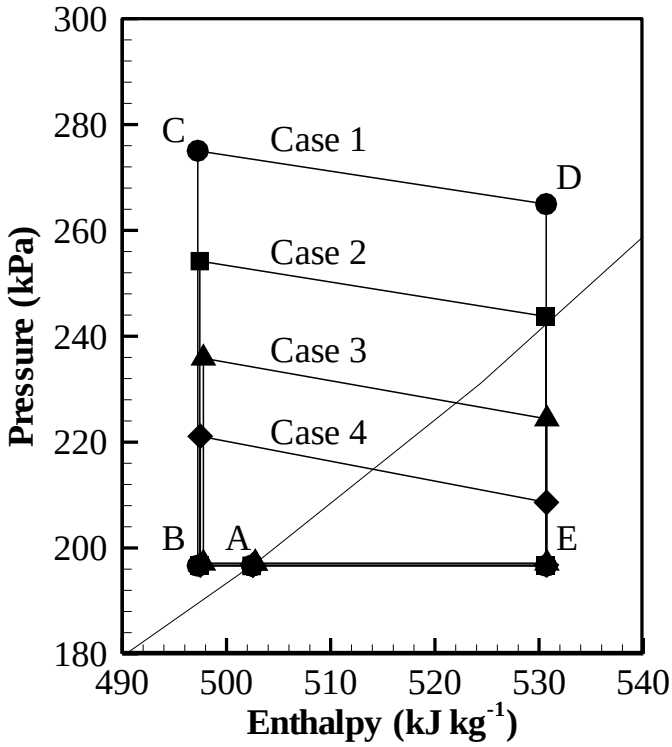

Fig. 3.4 Pressure-enthalpy diagram of water circulation

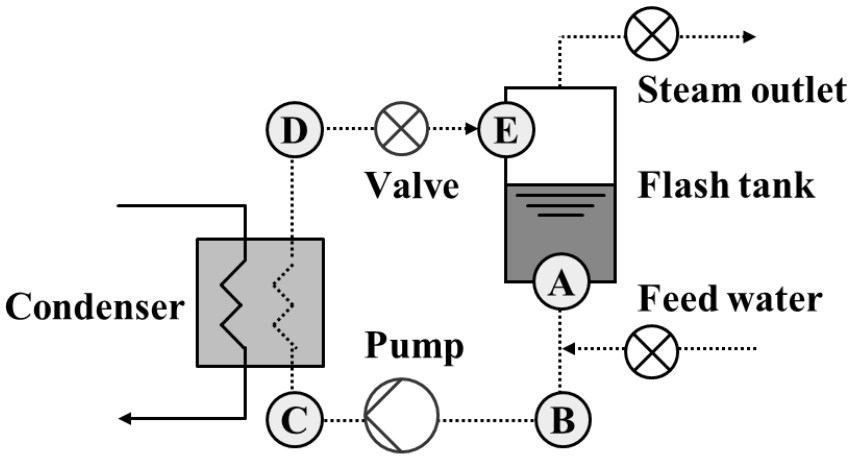

Fig. 3.5 Schematic diagram of water circulation

3.3.2 The mass flow rate of the water in evaporator

As shown in Figure 3.6, the evaporator water mass flow rate is changed from 300 to 1100 g s^{-1} when the degree of superheat of the evaporator outlet is fixed. In this experimental case, the saturated temperature of the refrigerant at the evaporator is fixed at 60℃. The increased water mass flow rate decreases the temperature difference of the water between the inlet and outlet temperatures of the evaporator from 4.8 to 1.4℃, and it increases the evaporating temperature of the heat pump from 50.3 to 53.7℃. In addition, the refrigerant mass flow rate increases from 45.0 to 50.6 g s^{-1}. The heat transfer rate in the evaporator is calculated as shown in Equations (3.4) and (3.5). The result shows an increase of $\dot{m}_{eva.wat}$ with the enthalpy difference of refrigerant and inlet enthalpy of water fixed, as well as with increased refrigerant mass flow and water outlet enthalpy.

$$\dot{Q}_{eva.ref} = \dot{m}_{ref} \times (i_{eva.ref.out} - i_{eva.ref.in}) \quad (3.4)$$

$$\dot{Q}_{eva.wat} = \dot{m}_{eva.wat} \times (i_{eva.wat.in} - i_{eva.wat.out}) \quad (3.5)$$

As the evaporator inlet temperature (heat source temperature) increases, the compression ratio decreases and the COP increases when the evaporator water mass flow rate is fixed. Even the refrigerant mass flow rate and compression work increase; as shown in Figure 2.7, COP increased due to the

increased condensing heat transfer rate. The increase of water mass flow rate decreases the difference in inlet and outlet water temperatures, but the evaporation heat transfer rate increases more quickly. Because the inlet and outlet enthalpy difference of the refrigerant is fixed, the mass flow rate of the refrigerant increases, which leads to an increase of compression work. The increased evaporation heat transfer rate and compression work lead to increases in condensing heat transfer rate and COP. The condensing heat increased by 11.3% and the steam generation rate increased from 2.7 to 2.9 g s^{-1}. The increase in water mass flow rate at the evaporator increases the condensing pressure and the evaporating pressure of the refrigerant.

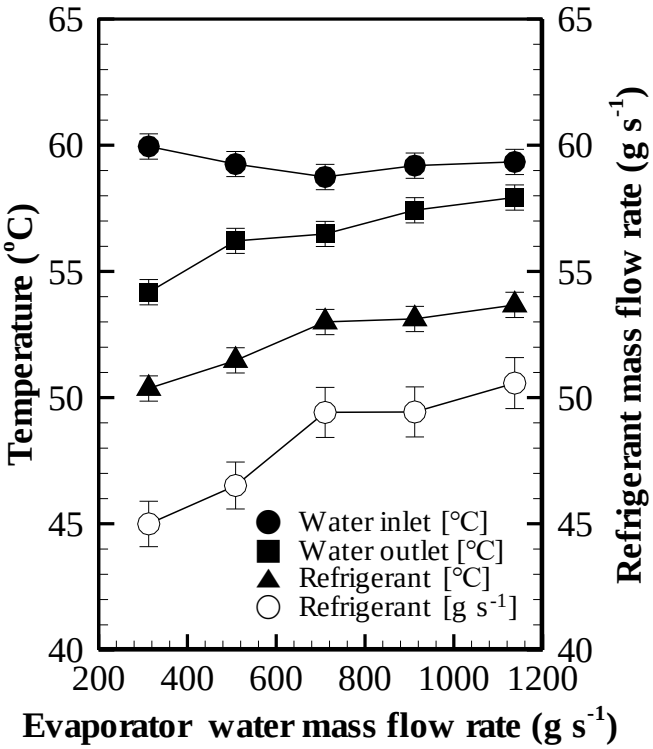

Fig. 3.6 Temperature and mass flow rate

according to water mass flow rate at the evaporator

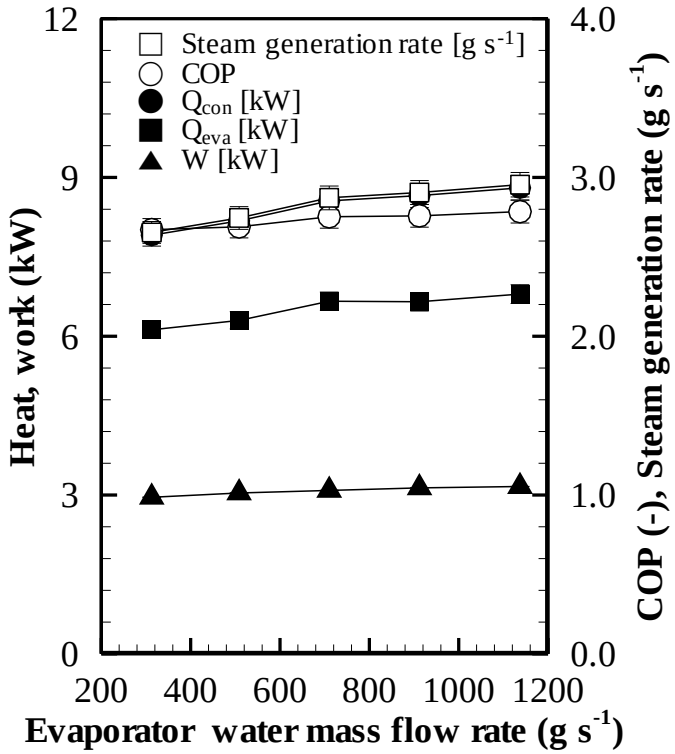

Fig. 3.7 Heat, work and COP according to water mass flow at the evaporator

(T_{eva} = 70°C, $\dot{m}_{ref}$ = 70 g s^{-1}, $\dot{m}_{con.wat}$ = 800 g s^{-1})

3.3.3 The pressure of the water in the flash tank

One can adjust the saturation temperature at the flash tank and the condenser outlet temperature by controlling the pressure of the flash tank. This also determines the condensation temperature of the heat pump cycle. As shown in Figure 3.8, the diagram varies greatly depending on the pressure of the flash tank. The COP at 120℃ was 3.24, and it is 2.95 (-9.1%) at 125℃ and 3.59 (+10.8%) at 115℃. The compression work changed according to the compression ratio. This is because the mass flow rate and heat transfer coefficient of the water is larger than the refrigerant, and the temperature of the refrigerant follows the water temperature at the condenser. As the refrigerant in the condenser becomes high pressure, the compressor is operated with a larger pressure ratio, so the compression work increases. The fixed DSC leads to the increased enthalpy of the refrigerant at the evaporator inlet. To make the same DSH, the evaporation heat was not needed as much, and thus the EEV opening was adjusted so as to allow for less refrigerant mass flow. Even though the change in enthalpy difference is large while the refrigerant mass flow rate changes along with the compression work, the variation of the condensation heat is less than 3%. As a result, the variation of steam generation rate (3.0 g s^{-1}) is less than 6%.

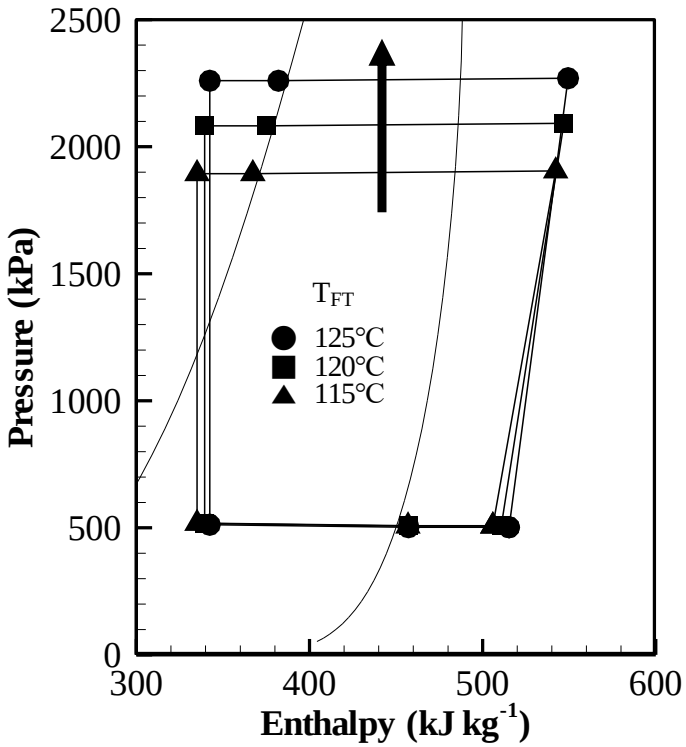

Fig. 3.8 Pressure-enthalpy diagram

by water saturation temperature at the flash tank

(T_{eva} = 70°C, $\dot{m}_{eva.wat}$ = 1100 g s^{-1})

3.3.4 The heat source temperature

Figure 3.9 shows the change in the pressure-enthalpy diagram for each heat source temperature. The condensation temperature also increased with the rise of the evaporation temperature even if the temperature of the flash tank was constant. The condensing temperature rises to make the temperature difference between the refrigerant and water higher as the heat of condenser increases. As the evaporation temperature increased, the enthalpy difference of condensation, evaporation, and internal heat exchange process decreased, but the heat amount increased since the refrigerant mass flow rate rises.

As shown in Figure 3.10, the EEV opening ratio was controlled so as to verify the system performance by the refrigerant mass flow rate at the compressor. The reduction of mass flow rate resulted in a decrease in evaporation temperature from 63.3 to 36.5℃ and an increase in DSH from 6.3 to 33.1℃. As the compression ratio increases, the compression work increases while both the condensation heat and evaporation heat both decrease and the COP decreases from 3.24 to 1.83. As the EEV is opened, the temperature difference between water and temperature decreases and the compression ratio decreases, so the evaporation temperature is expected to increase while the condensation temperature is expected to decrease. However, both the condensation and evaporation pressure were increased. The increase in the mass flow rate in the heat

exchanger makes it so that the temperatures of the two flows approach each other. As the expansion valve was opened, the difference between high and low pressures was reduced, but the pressure rise of the evaporator was greater than the decrease in pressure of the condenser. Therefore, both pressures increased even as the EEV was opened.

Figure 3.11 shows the variation of the heat transfer rate at heat exchangers and compression work per the refrigerant mass flow rate. As the refrigerant mass flow rate increases by opening EEV, the evaporating temperature increases and DSH decreases, and the COP increases from 1.83 to 3.24. The steam generation rate also increases from 1.2 to 3.3 g s^{-1}. However, lower DSH does not always produce better performance. R245fa is dry fluid and its saturation vapor enthalpy increases as pressure increases. The evaporation pressure rises linearly but DSH decreases rapidly. When the minimum unit opening of the expansion valve is opened further, the DSH becomes a negative value, and the refrigerant exits the evaporator in two phases. Since the mass flow rate of water in the heat exchanger is very large, the outlet temperature of the refrigerant coincides with the inlet temperature of the water. If the evaporator outlet is not superheated and becomes two phases, the evaporation temperature rises to the outlet temperature of the water. The temperature difference between the evaporating temperature of the refrigerant and the water reduces the amount of heat exchange.

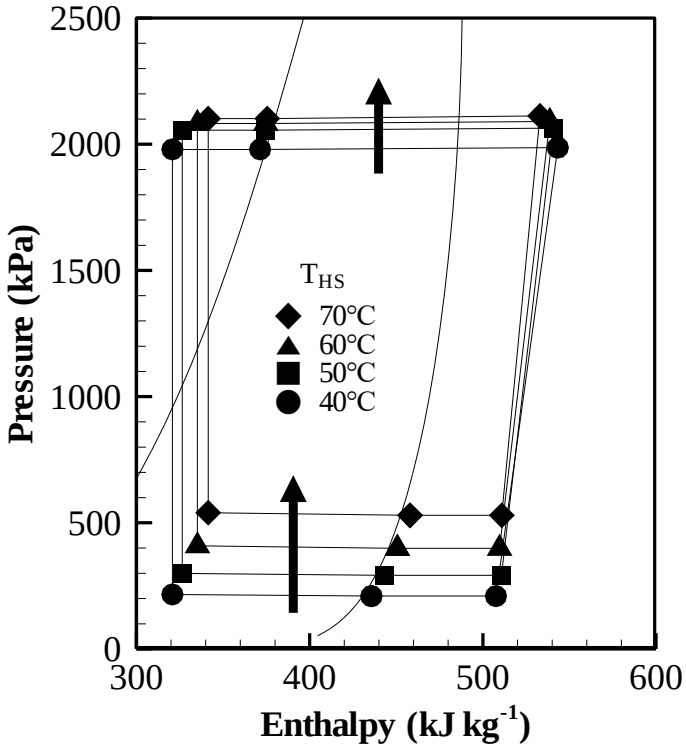

Fig. 3.9 Pressure-enthalpy diagram

by heat source temperature of the heat pump

(T_{FT} = 120°C)

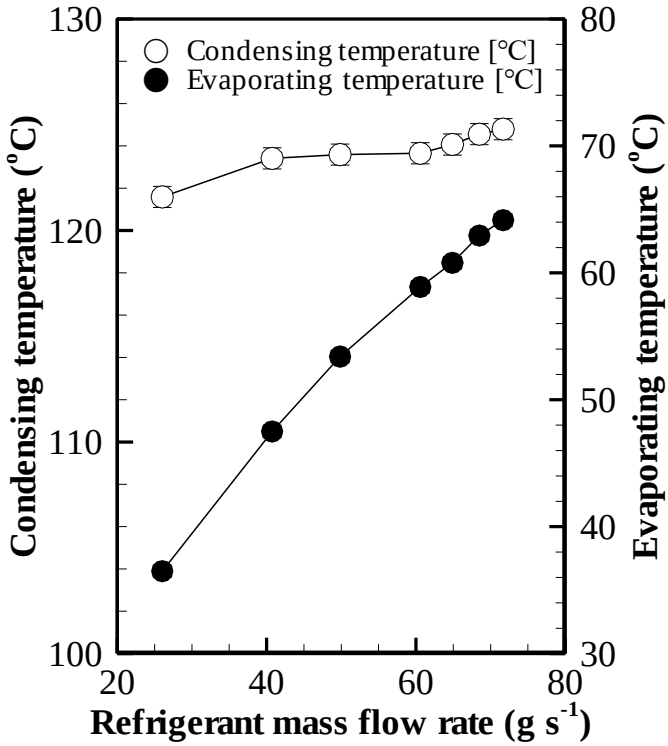

Fig. 3.10 Pressure-enthalpy diagram

by mass flow rate of the refrigerant

(T_{eva} = 70℃, $\dot{m}_{con.wat}$ = 800 g s^{-1}, $\dot{m}_{eva.wat}$ = 1100 g s^{-1})

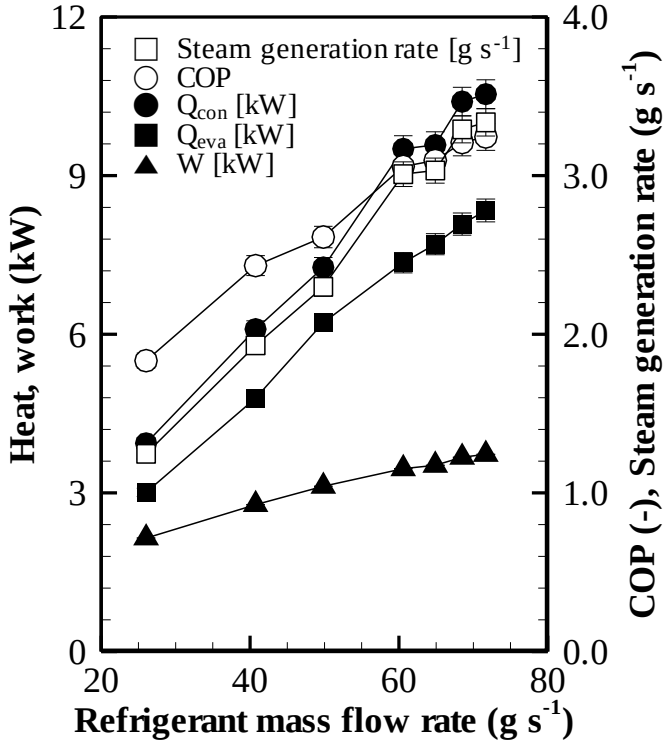

Fig. 3.11 Heat, work and COP

by refrigerant mass flow rate

(T_{eva} = 70℃, $\dot{m}_{con.wat}$ = 800 g s^{-1}, $\dot{m}_{eva.wat}$ = 1100 g s^{-1})

(Fixed DSH)

3.3.5 The capacity of IHX

As shown in Figure 3.3, the steam generation cycle with the internal heat exchanger (IHX) is compared to the basic cycle without IHX. In order to prevent wet compression, the basic cycle required a larger DSH than the IHX cycle, and DSH was controlled to be constant at the same temperature (12℃) so as to allow for comparison of the performance in the same operating conditions. When the heat source temperature is 60℃, the compression work, condensation heat, and COP are all increased by introducing IHX. The condensation heat increased by the enthalpy of the condenser inlet was increased by the low temperature part of IHX, and the evaporation heat increased by the enthalpy of the evaporator inlet was decreased by the high temperature part of IHX. The compression work increased only 6.2% when the DSH of the compressor inlet increases 12℃ to 64℃.

For heat source temperature of 70℃, the system performance according to the internal heat exchanger mass flow split ratio is shown in Figures 3.12 and 3.13. The internal heat exchanger mass flow split ratio is defined as the mass flow rate into the IHX over the mass flow rate at the compressor, as shown in Eq. (3.6). The mass flow rate at IHX was calculated as shown in Eq. (3.7). The refrigerant is branched at the evaporator outlet. The enthalpy of the refrigerant passing the IHX increases, and the enthalpy of the refrigerant passing the bypass line remains constant. The mixture of the two enters the receiver in front of the compressor, and its enthalpy is calculated by measured pressure and

temperature. The mass flow split ratio (rihx) was calculated through the following three enthalpies. The internal heat exchanger mass flow split ratio can be rewritten as the normalized IHX capacity.

$$r_{ihx} = \dot{m}_{ihx} \div \dot{m}_{comp} \quad (3.6)$$

$$\dot{m}_{ihx} = \dot{m}_{comp} \frac{h_{mix} - h_{eva}}{h_{ihx} - h_{eva}} \quad (3.7)$$

Figure 3.12 shows the pressure-enthalpy diagram when the condensing pressure and the evaporating pressure were kept constant. The evaporation temperature was set at the highest temperature when the heat source temperature is 70℃. The IHX cycle was operated with an evaporation temperature of 65℃ and a DSH of 5℃. The basic cycle was operated with an evaporation temperature of 60℃ and a DSH of 10℃. The DSH of the basic cycle is set to be higher so as to avoid potential liquid compression. The compression efficiency was kept similar for the same condensing and evaporating pressures, as shown in the figure. The steam generation rate, condensing heat transfer rate, evaporating heat transfer rate, compression work, and COP all increased. The steam generation rate increased 2.6 to 3.0 g s-1 with increasing mass flow split ratio. Increasing the amount of internal heat exchange with fixed DSH and DSC at the same compression ratio increases the heat transfer rate at the condenser and the evaporator. Unlike the IHX cycle, the basic cycle has a large DSH to prevent liquid compression, and this leads

to a lower enthalpy difference of evaporator.

As shown in Figure 3.13, when the EEV opening is fixed, the evaporating temperature, evaporating pressure, and refrigerant flow rate increase as the mass flow split ratio increases. By contrast, when the evaporation temperature and refrigerant flow rate are fixed, the EEV opening should gradually increase as the amount of refrigerant passing through the IHX increases. The reason for the change of the evaporation pressure is that the condensation temperature cannot be lowered below the inlet water temperature despite the change of the compression ratio. The refrigerant enthalpy at the evaporator outlet is similar to the inlet temperature of the water. However, the refrigerant enthalpy at the evaporator inlet changes with the amount of internal heat exchange. An increase in internal heat exchange increases the evaporator enthalpy difference.

An explanation is added about the change in the evaporation pressure. In the formula of the mass flow rate for expansion valves, the inlet density slightly increased as the DSC decreased. Thus, the outlet pressure also slightly increased.

$$\dot{m}_{ev} = C_d\sqrt{\rho_{in}(P_{in} - P_{out})} \tag{3.8}$$

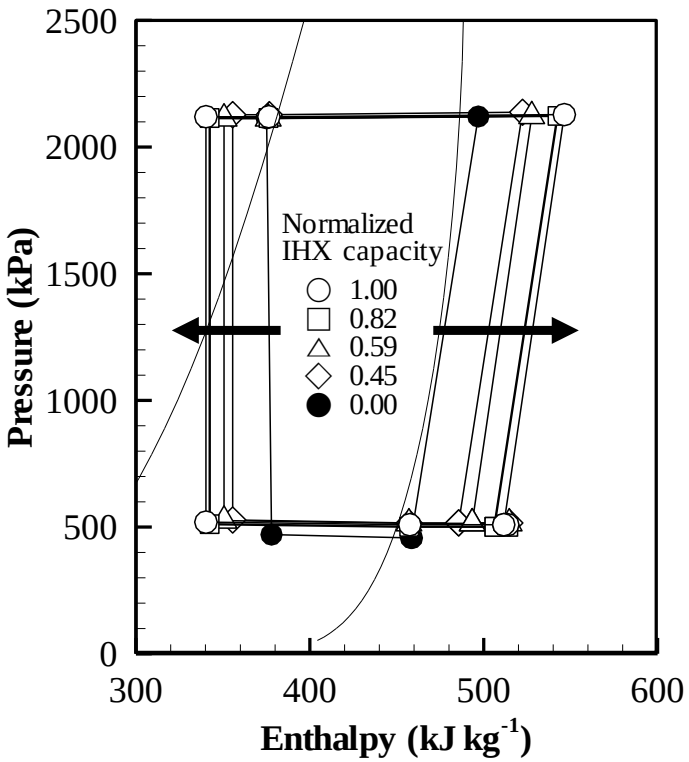

Fig. 3.12 Diagrams according to the IHX mass flow split ratio

(fixed evaporating pressure)

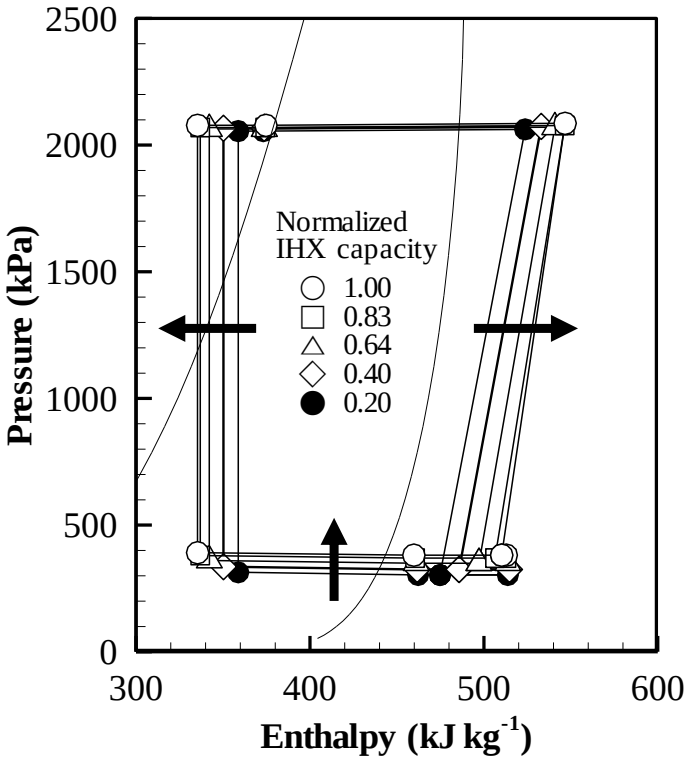

Fig. 3.13 Diagrams according to the IHX mass flow split ratio

(fixed EEV opening)

Figure 3.14 shows the evaporating heat transfer rate and condensing heat transfer rate both increase, and this leads to an increase in steam generation rate. The increase of the evaporating heat increased the evaporation temperature by reducing the temperature difference of water inlet and outlet. As the compression ratio increases, the enthalpy difference increases as well. The evaporator refrigerant mass flow rate remained constant, but compression work increased slightly. The increase in both heat transfer rates is greater than that of compression work, and the COP increases. As the mass flow split ratio increased, the steam generation rate increased 2.3 to 2.5 g s^{-1}. The reason for these phenomena is that the DSH of the refrigerant entering the compressor increases. As the density of the refrigerant entering the compressor decreases, the mass flow rate increases.

Figure 3.15 shows the change in COP when the IHX capacity is varied in different EEV opening. At the same EEV opening, an increase in the IHX capacity increases the evaporating temperature. As the IHX capacity rises, the heat amount in the condenser converges but the compression work increases linearly, so an optimal COP exists. Therefore, a strategy of bypassing some refrigerant flow rate is a method of using less compression work while obtaining the same amount of the condensing heat and the steam generation rate.

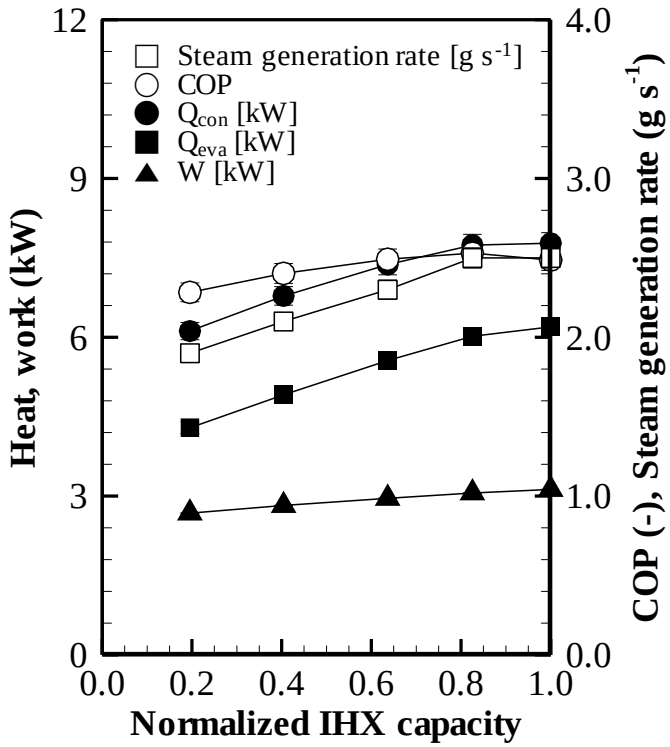

Fig. 3.14 Performance according to the normalized IHX capacity

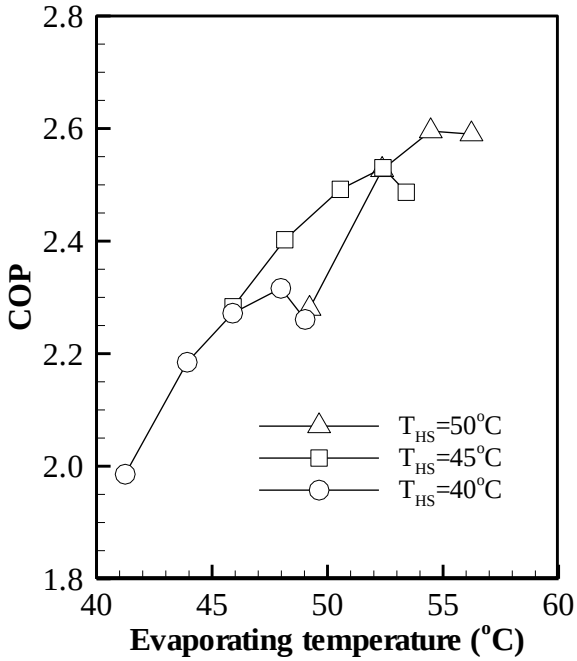

Fig. 3.15 COP according to the EEV opening and internal heat exchanger capacity

3.4 Operating efficiency of heat pump and boiler

Natural gas can be converted to electricity for the heat pump or be used as fuel for the boiler. Figure 3.17 compares the experimental steam generation rate through the SGHP and the theoretical steam generation rate through the conventional gas boiler. The heat pump cycle at the heat source temperature of 70℃ was used as a reference case. The amount of natural gas used in the power plant can be calculated by dividing the compression work of the reference cycle (3.1 kW) by the energy density of natural gas (50 MJ/kg) and the efficiency of power plant (50%) [86] (KEEI, 2018). The amount of steam generation by a gas boiler (1.7 g/s) can be calculated using the gas boiler efficiency (70%) [87] (IEA ETSAP, 2010).

As a result, under representative conditions, the heat pump cycle can make 35% more steam compared to the gas boiler using the same amount of natural gas. Additionally, the introduction of IHX could increase the amount of steam by 22%. Hence, the heat pump cycle with the internal heat exchanger can produce more than 64% steam compared to the gas boiler.

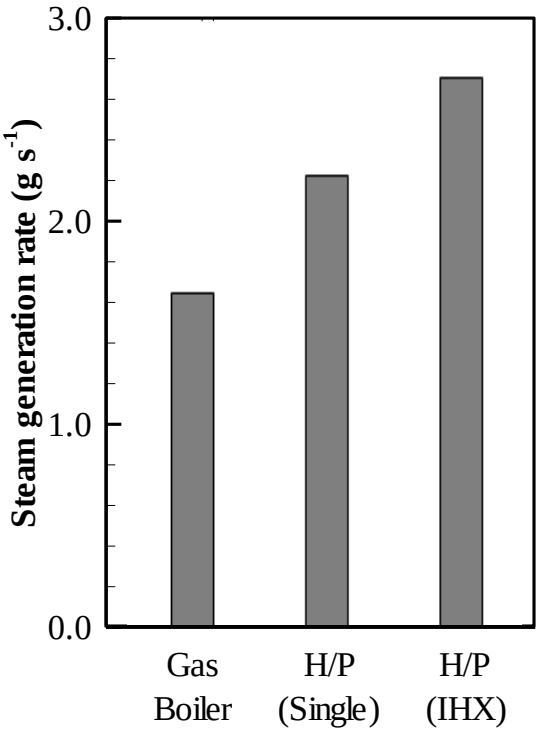

Fig. 3.16 Comparison of heat pump and boiler

3.5 Summary

This study is conducted in an attempt to improve the steam generation rate over the conventional steam boiler. To obtain operating characteristics, the effects of the mass flow rates of fluids, as well as the mass flow split ratio to the IHX were observed.

The condensation temperature of the heat pump and the steam temperature could be determined by controlling the pressure of the flash tank. Reducing the pressure of the flash tank rises the performance, but the performance growth rate decreases. By installing a valve between the condenser and the flash tank, water fluctuation can be prevented, and power consumption of the pump can be reduced, even when the amount of the steam generation is within the error range.

The mass flow split ratio of the IHX simulated the capacity of IHX. As the capacity of IHX increases, performance of the system increases. The increase in the capacity of IHX also rises the mass flow rate and the evaporation pressure of the refrigerant. Reducing the refrigerant flow bypassing IHX performs a similar function as increasing the EEV opening.

The SGHP cycle shows 35% more steam compared to the boiler system from the same amount of natural gas. The adoption of IHX increased steam amount by 27 to 31%, depending on the EEV opening. [88]

Chapter 4. Transient behavior of the high temperature heat pump with flash tank operation

4.1 Introduction

Conventionally, the steam boiler is used for making industrial steam. A boiler that circulates or passes water through a heat source is called a water-tube type boiler. The opposite form is called a fire-tube type boiler. In a water-tube type boiler, water is introduced into the drum, and circulated through the furnace and the drum. Examples of water-tube type boilers include coal-fired boilers, steam generators of the nuclear plant, and desalination plant.

The following references focused on modeling of water circulation and water level control for the steam boiler. Bahadori et al. [69] provided a predictive tool for the blowdown system that removes the impurity of the steam drum. The tool is verified by experiment. Zhou et al. [70] developed a coordinated control system of steam turbine regenerative system. The authors proposed an improved strategy based on extraction system. Chandrasekharan et al. [71-72] formulated simple transfer function models for integrated boiler units. The model is based on first principle laws and validated with the plant data. The authors also compared three multivariable-control strategies. The authors suggested integrated multi-loop control rather than individual control units. Sunil et al. [73-74] combined a lumped model of drum and distributed

model of the evaporator. The authors compared a model with two other non-linear models. The authors designed a robust control system used the quantitative feedback theory. A comparative analysis is used to show the performance. Satyavada et al. [75] proposed a monitoring approach that extends the operating regime for which monitoring is possible.

There is also dynamic model of other type of boilers. Sedic et al. [76] suggested a nonlinear dynamic model of the natural circulation steam boiler based on the physical laws of conservation. The authors anticipated the proposed model is easily adapted to the case of other boilers with only key parameters. Liu et al. [77] presented a model of once-through boiler-turbine unit. The change of phase transition position is avoided to simplify the model. Tognoli et al. [78] developed a FEM (Finite element method) based model with a PID (Proportional, Integral, Differential) controller. The authors suggested cumulative efficiency and pressure deviation. Beyne et al. [79] developed both a steady state and dynamic heat transfer model

Heat pumps could save primary energy usage compared to boilers and could utilize waste heat of industrial field. However, the temperature range of the industrial heat pump has been less than 100℃. The dynamic modeling of the heat pump and the water tank is as follows. Sanaye et al. [80] performed the modeling of gas engine driven heat pump during startup. The modeling included transient heat transfer equations, and validated by the empirical results. Koury et al. [81] formulated the models for heat exchangers and capillary tube.

The instability is reduced through the convergence process. Faria et al. [82] presented dynamic behavior of CO_2 heat pump with solar evaporator. The behavior of the system is influenced by the dynamics of the heat transfer. Qiao et al. [83] proposed a distributed-parameter dynamic heat exchanger model integrated with frost formation. An iteration-free approach is suggested to solve non-linear pressure drop. Liu et al. [84] showed dynamic optimal strategy for charging of thermal storages coupled with CO_2 heat pump. The suggested strategy can search the optimal COP in transient state. Deutz et al. [85] combined a zonal tank model approach with a grey box heat pump model.

Figure 4.1 shows the schematic diagram of the steam generation heat pump system. The process of the steam generation heat pump is similar to the process of water-tube type boilers that make steam. The water circulates through the flash tank and the condenser of the heat pump cycle. The condenser of the heat pump acts as a furnace. The economizer to heat the water before the flash tank is not existed, but hot water from a heat source of the heat pump can be supplied. Circulation line of SGHP has no separate name such as downcomer and riser. The superheater to heat the steam after the flash tank is not existed, but the steam can be mechanically recompressed by adding a device (MVR, mechanically vapor recompression).

In this chapter, transient behavior of the heat pump with the flash tank was observed and compared with the experimental data.

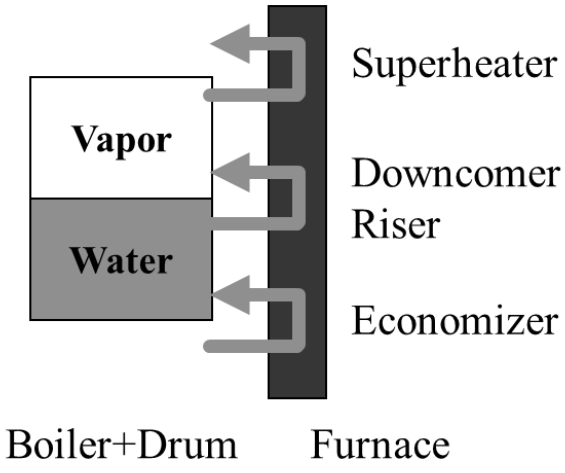

(a) Boiling by furnace and drum

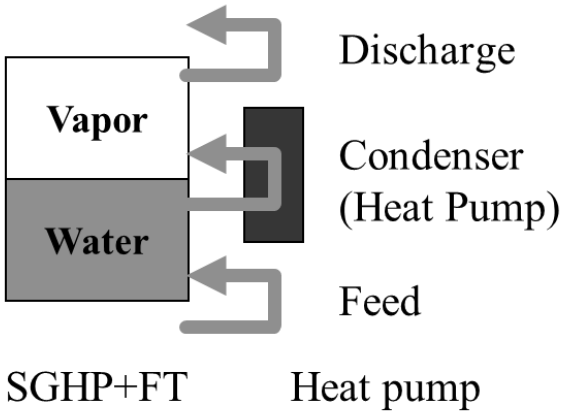

(b) Boiling by heat pump and flash tank

Fig. 4.1 Schematic diagram of water boiling

4.2 Dynamic modeling

The steady state means no change, and the quasi-steady state is a state where the amount of change is very small and can be ignored in equilibrium. Dynamic state means change state, and transient state means the middle state between two equilibrium states. This section is Transient modeling because it simulates the dynamic behavior between two equilibrium states.

Mathematically, dealing with PDEs that depend on more than one variable is called a distributed model, and dealing with ODEs that are driven by a single variable is called a lumped model. So, the accumulator and the heat exchanger modeling covered in this section is a lumped model. Each control volume of the heat exchanger has own density and enthalpy of the refrigerant and the secondary fluid. As the density increases or decreases, the refrigerant accumulates or falls out. It is assumed that there is only one pressure in the heat exchanger. After condenser calculation, converge the condensing pressure so that the outlet pressure and expansion valve inlet pressure are the same.

Calculating sequential process is called time integration. Difference methods include the front-rear-center method. Explicit analysis calculates later state from current state. Implicit analysis solves from the current state and the later state. In this case, only the initial condition is given and the behavior values of the next time point are obtained sequentially, so the Explicit Euler backward difference is used.

The explicit method uses time-steps consistently, which is called global time stepping. The decision of the time-step (dt) follows the Courant–Friedrichs–Lewy condition (CFL condition) for numerical stability, or solution convergence. This is equivalent to equation (4.1). The formula of the time interval (dt), speed (u), element size (dx) must be less than the number of Courants. For simple primary accuracy, the number of Courants is one.

If the CFL condition corresponds to the mass storage equation of the control volume, it can be regarded as a change in mass and a change in mass flow rate. By setting dt (right side of the equation) constant, and left side of the equation was checked throughout the analysis. The dt has the stability of analysis when less than 0.2 seconds.

$$\frac{u\Delta t}{\Delta x} \leq C = 1 \tag{4.1}$$

$$\frac{m(t)-m(t-dt)}{\dot{m}_{in}(t)-\dot{m}_{out}(t)} = dt_{cal} \leq dt \tag{4.2}$$

Transient modeling is an analysis method that assigns the value of every cycle to the next step, unlike steady-state modeling. As shown in Figure 4.2, the value from step i is used to calculate step i+1. For the convergence of condensing and evaporating pressures, the calculation of expansion device and accumulator was added. The condensing pressure was determined by the agreement of the mass flow rates of the condenser outlet and the expansion

valve. The evaporating pressure was determined by the agreement of the mass flow rates of the compressor and accumulator.

$$\dot{m}_{ev} = C_d\sqrt{\rho_{in}(P_{out} - P_{in})} \tag{4.3}$$

$$\dot{m}_{ac} = \dot{m}_{in} - \frac{(\rho_{out} - \rho_{in})V_{ac}}{dt} \tag{4.4}$$

The equations contain time term. As in Equation (4.3), the mass flow rate of the expansion valve outlet was determined according to the difference between the opening and the inlet pressure of the valve. It is assumed that the enthalpy of the expansion valve before and after does not change. As in Equation (4.4), the mass flow rate was determined according to the density change. If the internal enthalpy of the accumulator is in the two-phase state, it is assumed to discharge saturated vapor state of the refrigerant. The accumulator is a device that prevents liquid from entering the compressor.

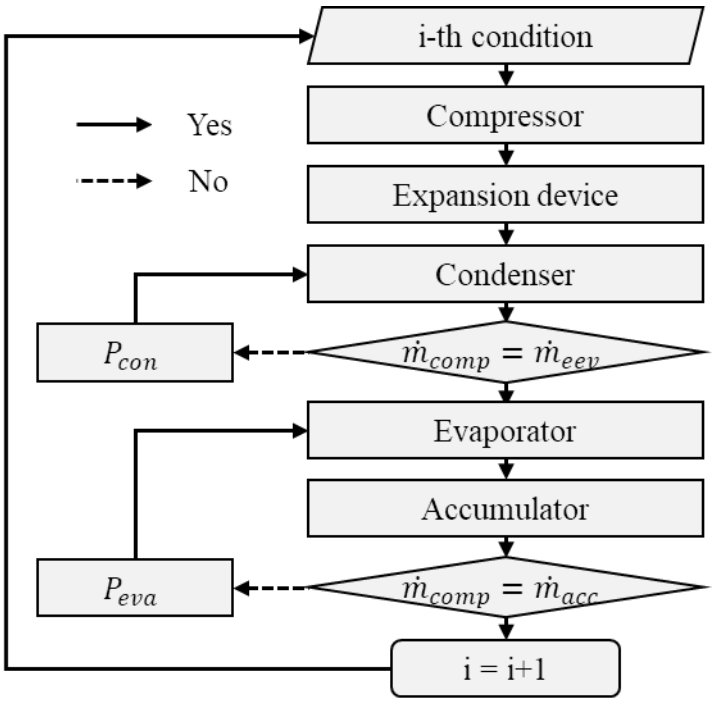

Fig. 4.2 Flow chart of transient single cycle calculation

Unlike a heat source reservoir with a fixed temperature, the water in the flash tank, which receives heat from the condenser, continues to rise in temperature. The enthalpy of the water increases only up to 100℃, and the pressure also rises after the water starts to boil. When the pressure of the flash tank reaches the target value, steam is discharged, and the same amount of the water is feed to mass conservation.

Pressurization of the flash tank was calculated on the assumption that the quality, i.e. the mass ratio of liquid and vapor, is constant even with increasing enthalpy. The change in pressure of the flash tank after the discharge of steam was calculated on the assumption that the level of water level, that is volume ratio, was constant. The calculation process of the flash tank is shown in Figure 4.3.

The amount of steam discharged depends on the amount of heat received from the condenser, as shown in Equation (4.5). In an actual experiment, a temporal error occurred while the discharged mass flow rate of steam and the time of controlling the mass flow rate of the feed water.

$$\dot{m}_{steam} = Q_{con} \div (h_{FT-V} - h_{feed}) \quad (4.5)$$

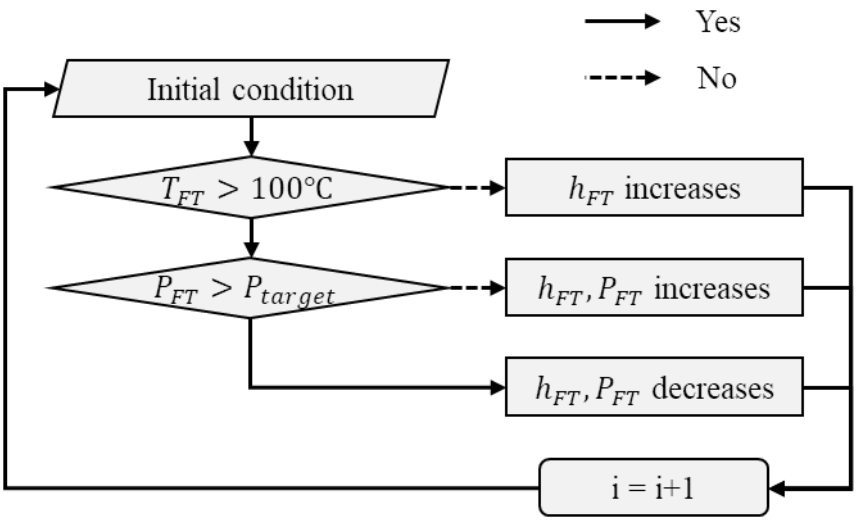

Fig. 4.3 Flow chart of the water circulation

between the condenser and the flash tank

4.3 Results and discussion

4.3.1 Start-up process

After modeling the system, the modeling is needed to evaluate and validate by the experimental data. The experimental data were presented to record the parameters and to compare the modeling output. The experimental setup described in the previous chapter was used. The dynamic operation of the system from the starting-up until reaching the steady state was investigated. The time consumed until the experimental setup becomes steady-state is about 30 minutes (2000 seconds).

The starting-up process can be divided into 4 stages based on the temperature of the refrigerant and the water. Firstly, the temperature starts at room temperature and is separated into high and low temperature (200 seconds). As a second stage, the condensing temperature of the refrigerant passes through the fixed water temperature in the heat source (800 seconds). As a third stage, the water in the flash tank starts to boil at 100℃ (1200 seconds). As the last stage, the temperature of the water reaches a steady-state of the target temperature (2000 seconds). The third to last stage is as same as flow chart of the water circulation as shown in Figure 4.3.

Figure 4.4 shows the pressure of the fluids (Refrigerant, water) according to time variation. The condensing and evaporating pressure of the refrigerant rises in the form of a straight line at stage 1, a curve at stage 2, and shows the vibration after water boiling. The flash tank pressure of the water shows a sharp increase from stage 3 when the water is boiling. Each pressure is being steady-state at stage 4. The pressure of the heat source reservoir was kept constant at atmospheric pressure. The difference between the experiment and the modeling is due to the difference in the the time of the water in the flash tank is heated to the two-phase.

Figure 4.5 shows the change in temperature over time for fluids. The water temperature of the flash tank rises along with the condenser refrigerant temperature. The refrigerant temperature of the evaporator follows the water temperature of the fixed heat source. Unlike water in heat source of constant temperature, the water in the flash tank is heated from the feed water. Around 900 seconds, the water temperature of the flash tank reverses the water temperature of the heat source. As the water boils around 1200 seconds, the temperature, the pressure changes slightly. This change is more clearly seen in the change in mass flow rate.

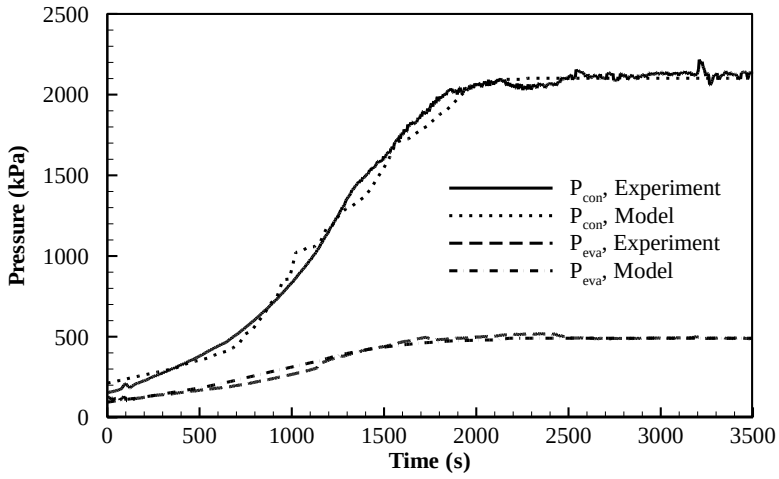

(a) Refrigerant (condenser, evaporator)

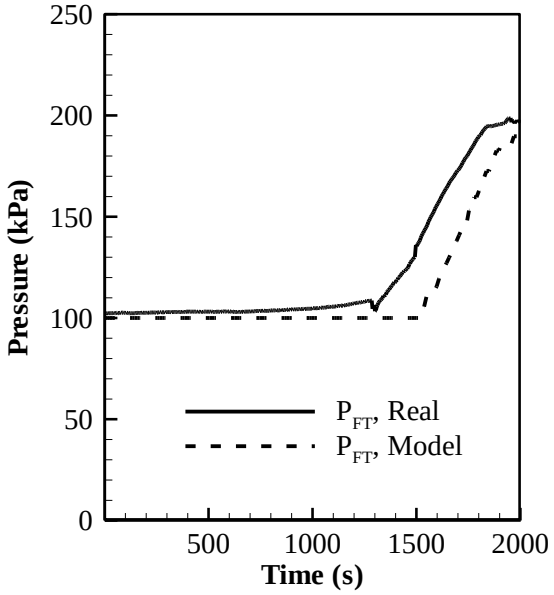

(b) Water (flash tank)

Fig. 4.4 The pressure change of the fluids in starting-up

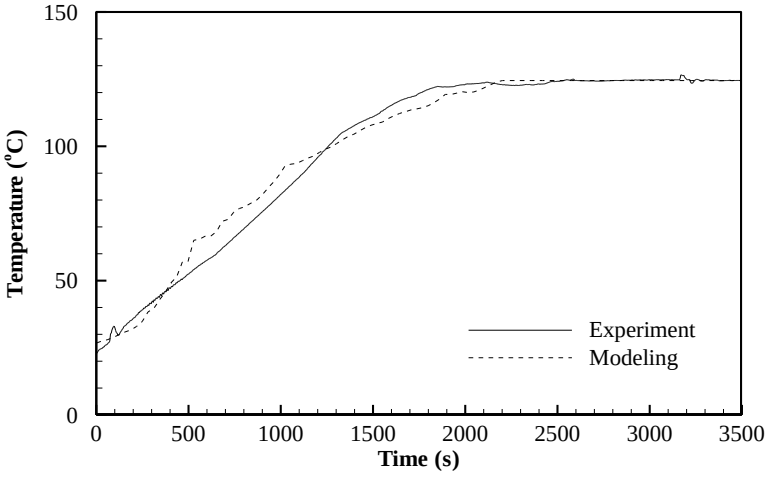

(a) Refrigerant (condenser, evaporator)

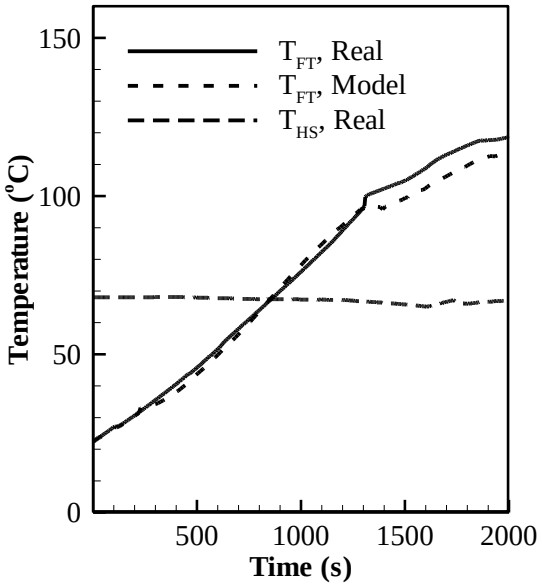

(b) Water (flash tank, heat source)

Fig. 4.5 The temperature change of the fluids in starting-up

Figure 4.6 shows the change in the mass flow rate of the fluids. The mass flow rate of the water between the evaporator and the heat source was kept constant. The mass flow rate of the refrigerant rose in a straight-line shape and showed a horizontal line when it reached the target value. The reason why the two values differ greatly is that the model value uses the value from the expansion valve, and the experimental measured data was from the compressor inlet. The mass flow rate varies depending on the change in density for each position.

The mass flow rate of the water between the condenser and the flash tank showed one step lowering after water boiling. The phenomenon is due to the change in the net positive suction head (NPSH). The water pump has its required NPSH value. Available NPSH should be higher than the required NPSH to avoid cavitation in the pump. If the water boils in a sealed water tank, the pressure of the water surface (P_s) is equal to the saturated vapor pressure (P_v). Therefore, the value of available NPSH is equal to the height from the pump to the water surface (h_s) minus the friction loss head of the pipe (h_f). As the water boils and finds a new equilibrium point, the mass flow is lowered, and the steady-state is maintained again.

.

$$\mathrm{NPSH_{av}} = \frac{1}{\gamma}(P_s - P_v) + h_s - h_L \qquad (4.6)$$

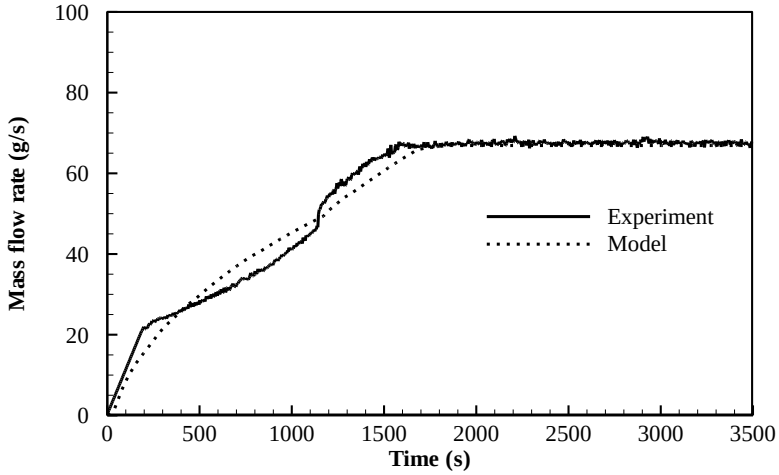

(a) Refrigerant

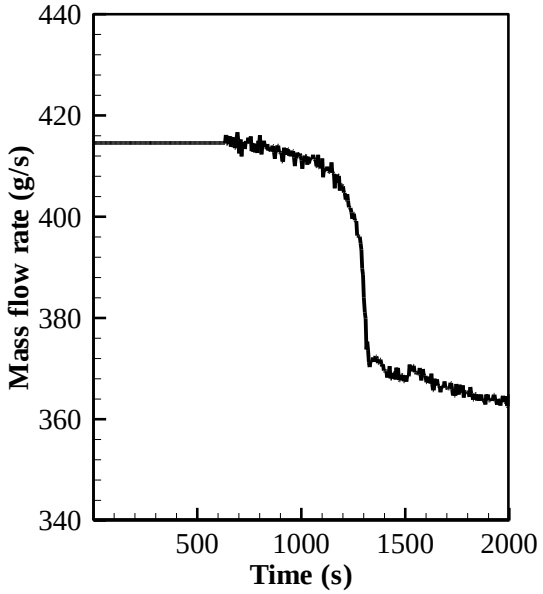

(b) Water (flash tank to condenser)

Fig. 4.6 The mass flow rate change of the fluids in starting-up

The changed in the pressure-enthalpy diagram of the refrigerant based on the measured temperature and pressure is shown in Figure 4.7. The refrigerant temperature of the evaporator outlet was fixed at the heat source temperature, and the DSH was decreased as the evaporation temperature increased. The refrigerant heated from the evaporator exchanges heat with the refrigerant at the outlet of the condenser at the IHX and is slightly cooled. When the condensation temperature becomes equal to the heat source temperature, the internal heat exchange amount becomes 0, and the appearance is the same as the single cycle. As the condensation temperature becomes higher, the effect of internal heat exchange is generated. The phase of the condenser outlet became two-phase when the final steady-state.

The heat exchange rate in the internal heat exchanger is initially negative, as shown in Figure 4.7. This is because the temperature of the feed water entering the condenser is lower than the temperature of the heat source entering the evaporator, as shown in Figure 4.5 (b). As a result, the internal heat exchanger becomes a factor degrading performance until the heat source temperature and the heat sink temperature reversed. Therefore, it is recommended not to use the internal heat exchanger at the start. Alternatively, it is recommended to feed water in the condenser at the same temperature as the heat source.

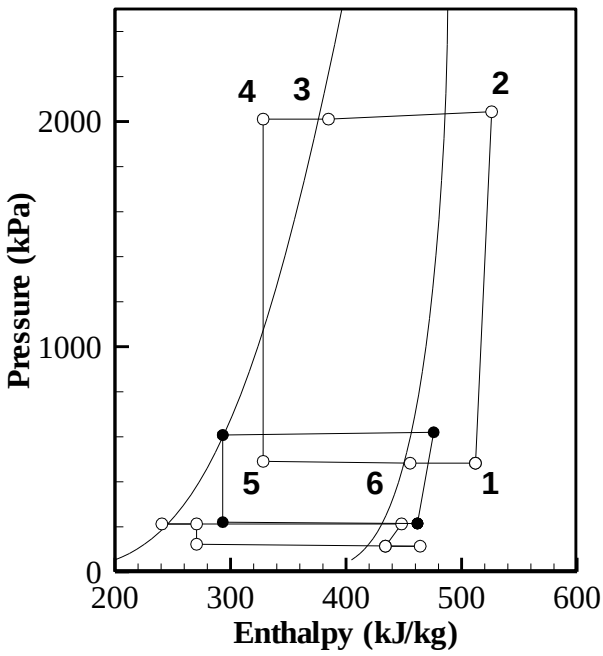

Fig. 4.7 Pressure-enthalpy diagram of the refrigerant in starting-up

(1: Compressor inlet / 2: Condenser inlet / 3: Condenser outlet /

4: Expansion valve inlet / 5: Evaporator inlet / 6: Evaporator outlet)

Figure 4.8 shows the change of the pressure-enthalpy diagram of the boiling water in the flash tank. The bottom left point of the cycle means the saturated liquid state of the water at the bottom of the flash tank. The water is pressurized by the pump, and receives heat from the condenser, increases the enthalpy and is decompressed. The water returns to the flash tank and is depressurized by the valve and become a two-phase state. The pressure of the flash tank is slightly increased by the generated steam, and when the water reaches the boiling point, the pressure rises rapidly.

The behavior of the water circulating the condenser and the flash tank differs greatly from that of the heat pump. An example of the design process of the flash tank is as follows. Firstly, the temperature of the waste heat determines the amount of the condensing heat. The compression work is determined according to the expected COP, and the compressor with appropriate speed and reciprocating volume is chosen. The amount of generated steam is determined by the condensing heat, and the mass flow rate of the feed water is also determined. The size of the flash tank is usually 15 minutes of the mass flow rate of the feed water. The mass flow rate of the water circulating causes the flash tank to be replaced in 10 seconds. Once the circulating mass flow rate is chosen, the required NPSH of the pump is known, thereby determining the height of the flash tank relative to the condenser.

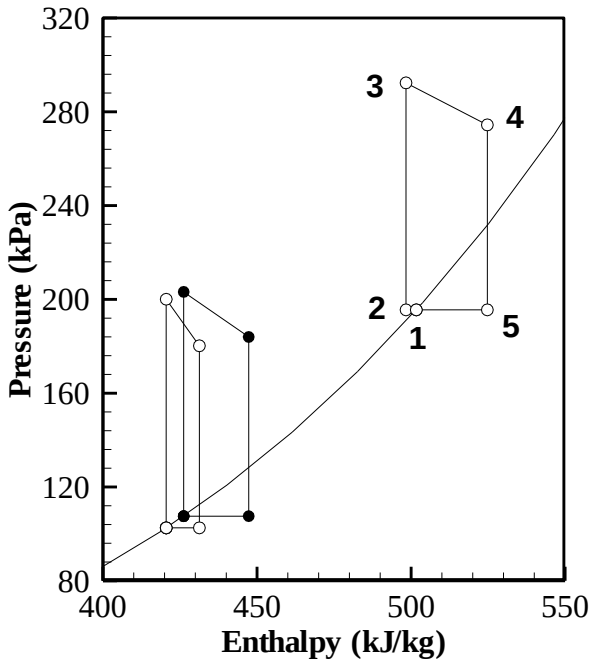

Fig. 4.8 Pressure-enthalpy diagram of the boiling water in starting-up

(1: Flash tank outlet / 2: Mix with the feed water / 3: Pressurized /

4: Condenser outlet / 5: Return to the flash tank)

4.3.2 Behavior by the change of flash tank pressure

Figure 4.9 and 4.10 shows the transient responses of the pressure and temperature of the heat pump system according to the pressure of the flash tank. The saturation temperature of the flash tank varied from 115 to 120, and from 120 to 125℃. Except the state dealing in the figure, the experiment and modeling shows steady-state. As the demand of the steam temperature changes, the flash tank should be pressurized, and the water level and saturation temperature in the flash tank change together. Since both the temperature and pressure of the secondary fluid side before and after the condenser change, the heat pump system also changes accordingly as the steam demand changes. The trend of the system is compared to the result of the simulation.

Figure 4.9 (a) shows the change of the condensing pressure. Unlike the oscillation in the experimental results, the modeling value produced a gentle curve. Figure 4.9 (b) shows the change of the evaporating pressure. The evaporation pressure required a large amplitude for the change. The amplitude means that the refrigerant mass arrangement in the components is changed in the process of change. In modeling, this process went smoothly and the amplitude was not large. This big difference is due to the liquid state refrigerant in the pipe. At the second steady-state, the evaporation pressure also increased slightly like the condensation pressure. As Figure 4.10 shows, the change in temperature also follows the change in pressure.

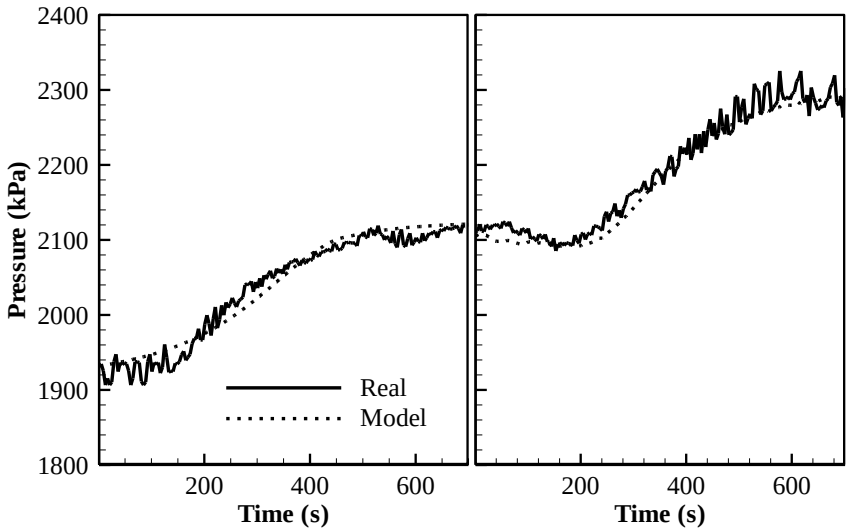

(a) Condensing pressure (refrigerant)

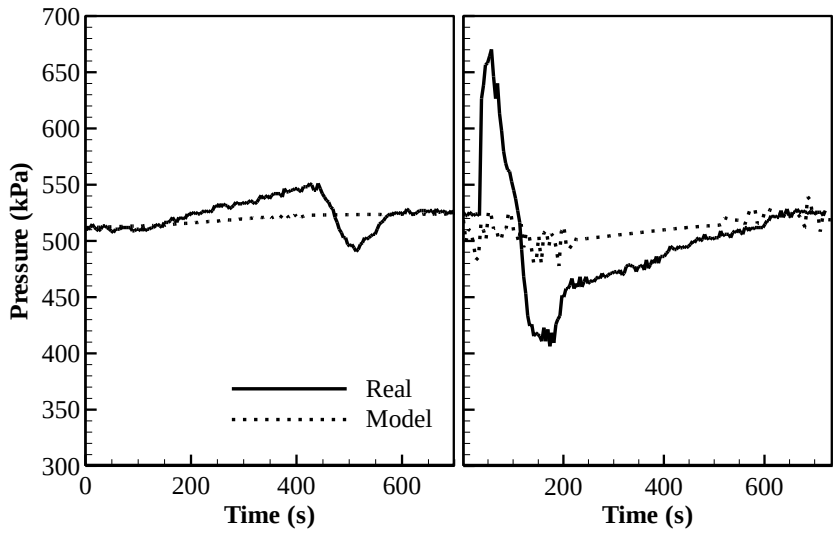

(b) Evaporating pressure (refrigerant)

Fig. 4.9 Changes of the pressures of the heat pump system

due to change of the flash tank pressure (115→120, 120 →125℃)

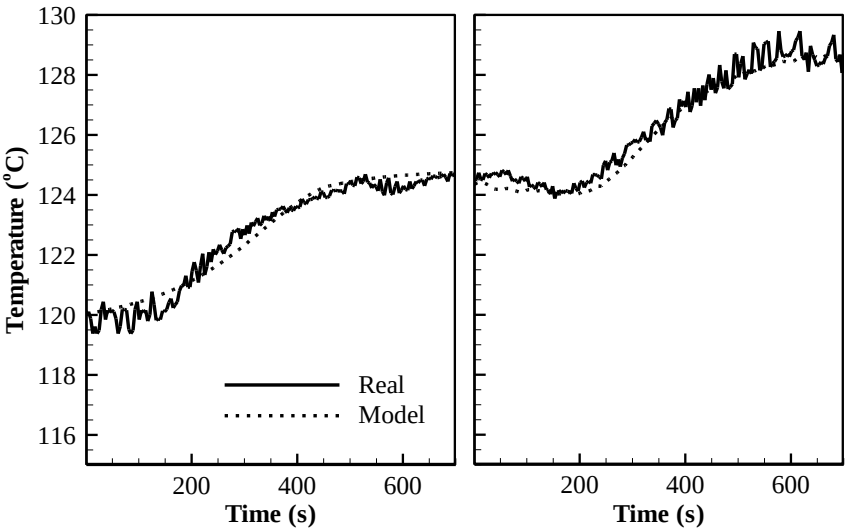

(a Condensing temperature (refrigerant)

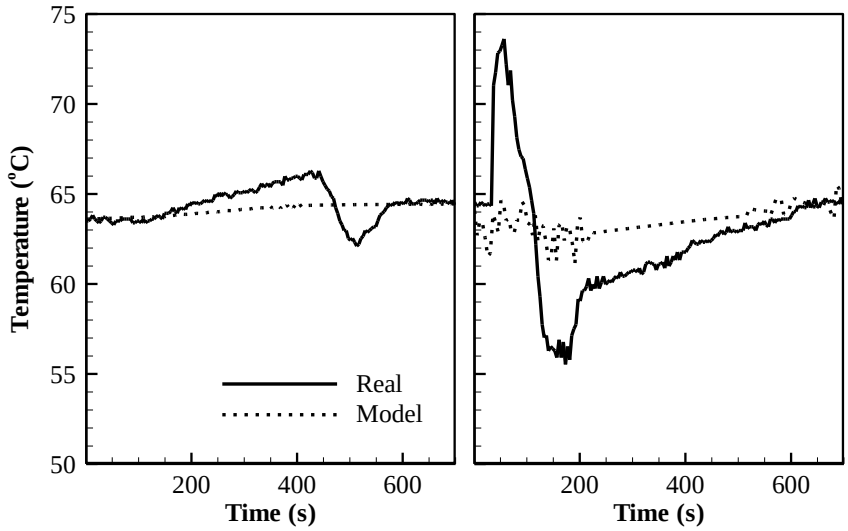

(b) Evaporating temperature (refrigerant)

Fig. 4.10 Changes of the temperature of the heat pump system

due to change of the flash tank pressure

By closing the outlet valve of the flash tank and increasing the pressure of the flash tank, high-temperature steam can be generated. The condensing heat from the heat pump remains the same, but energy is used to heat the feed water to a higher temperature, reducing the amount of steam produced. Therefore, to maintain the mass flow rate of the steam generated while producing high-temperature, the condensing heat must be increased. Therefore, the temperature and mass flow rate of the steam is determined according to the heat source temperature. Table 4.1 shows the temperature and mass flow rate of the steam that can be made from the same condensing heat.

In addition to the expansion valve in the heat pump, a variable that can be changed is the rotational speed of the compressor. The relative change of the main variables when the compressor speed is increased is shown in Figure 4.11. The compression work and the mass flow rate of the refrigerant increase, but the condensing heat does not change significantly. It can be seen that the condensing pressure remains unchanged and the evaporating pressure and temperature is lowered. Thus, changing the opening of the expansion valve is an advantageous strategy because it has the same effect while using the same compression work.

Table 4.1 Expected steam generation rate

due to the heat source temperature

T_{HS} (°C)		36.50	47.50	53.41	58.90	64.16
$\dot{m}_{ref}$ (g/s)		26.03	40.74	49.84	60.59	71.68
T_{FT} (°C)	105	1.66	2.60	3.18	3.86	4.57
	110	1.65	2.59	3.17	3.85	4.56
	115	1.65	2.58	3.16	3.84	4.54
	120	1.64	2.57	3.15	3.83	4.53
	125	1.64	2.57	3.14	3.82	4.52
	130	1.64	2.56	3.13	3.81	4.51
	135	1.63	2.55	3.13	3.80	4.49
	140	1.63	2.55	3.12	3.79	4.48

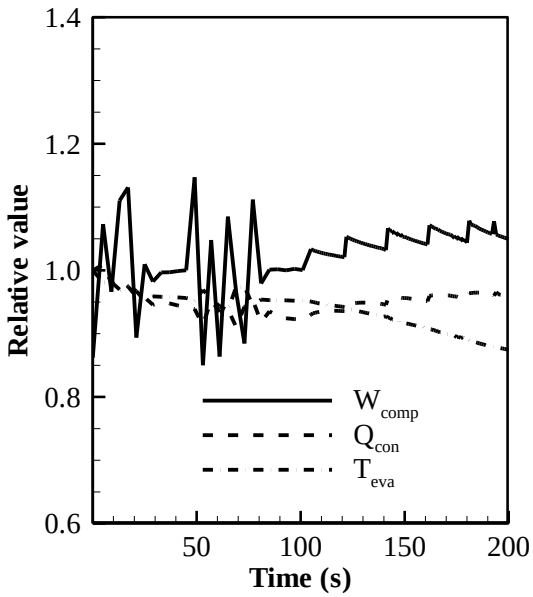

Fig. 4.11 Relative change of values due to change of compression speed

4.3.3 Behavior by the change of heat source temperature

Figure 4.12 shows the transient responses by the continuous cooling heat source. Steam generation heat pump utilizes industrial waste heat as its heat source. Unlike the conventional steady-state studies, in practice, the temperature of the heat source reservoir is constantly decreasing. The temperature of the heat source reservoir cools to 40℃ which is the allowable temperature for discharge to river or ocean. Therefore, the heat pump system should respond according to the heat source reservoir that continues to cool.

Even if the heat source temperature falls, change of the heat pump and the flash tank are insignificant as long as the heat source temperature is higher than the evaporation temperature. However, if the heat source temperature is less than or equal to the evaporation temperature, two-phase refrigerant will come out of the evaporator outlet and liquid refrigerant may enter the compressor. By reducing the opening of the expansion valve and continuously lowering the evaporation temperature, the system can cope with the cooling heat source temperature.

However, as mentioned earlier, closing the expansion valve reduces the refrigerant mass flow rate. It causes reduce of the condensing heat and steam generation rate. As Table 4.1 shows, lowering the temperature to generate the same amount of steam is an ineffective strategy.

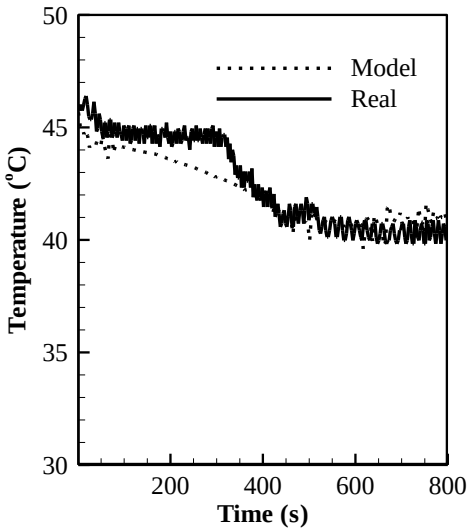

(a Evaporating temperature of the refrigerant

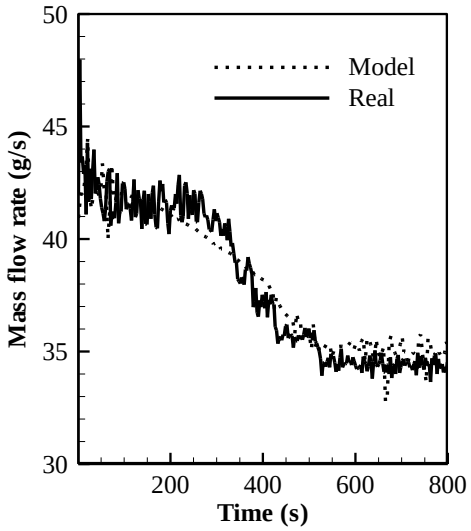

(b Mass flow rate of the refrigerant

Fig. 4.12 Changes of the heat pump system

due to closing the expansion valve

4.4 Summary

In this study, the dynamic behavior of heat pump system with the flash tank was investigated and compared with the experimental study. The study of transient behavior is necessary because the thermal storage-discharge of the condensing heat in the flash tank and steam generation were all related with time term. Additional model of components was added and the flow chart of analyzing is modified.

The start-up process can be divided to four stages by the temperature of water in the flash tank and the heat source. The heat exchange rate in the internal heat exchanger is initially negative. Therefore, it is recommended not to use the internal heat exchanger at the start. Alternatively, it is recommended to feed water in the condenser at the same temperature as the heat source.

When the flash tank pressure is changed, the pressures of the refrigerant in the heat pump system also changed. To maintain the mass flow rate of the steam generated while producing other temperature, the condensing heat need to be changed. The mass flow rate of the refrigerant can be modified by opening of the expansion valve.

When the heat source temperature is cooled, the evaporation temperature also should be cooled to avoid liquid compression. By closing the expansion valve, the mass flow rate of the refrigerant decreased and the condensing heat also decreased. It causes reduce of steam generation rate.

Chapter 5. Concluding remarks

Steam generation accounts for a large amount of energy consumption in the industrial sector. In addition, industrial waste heat (40 to 80 ℃) lower than useful hot water and higher than the discharge allowable temperature is discharged through cooling. High-temperature heat pump is recently emerged as an alternative to making useful steam and to cooling waste heat as the heat source. Conventionally, research has been conducted on the type of refrigerant, the configuration of the system, and modeling that simulates steady-state. R245fa in the refrigerant, the application of the internal heat exchanger in the configuration of the system is known to increase the efficiency.

However, the research on the effects of changing the configuration of the internal heat exchanger and transient-state modeling were limited. Unlike generating hot water, steam generation can vary in properties depending on its pressure and mass flow rate. Therefore, a model for dynamic behavior is needed. To suggest a proper operation method for steam generation heat pump, both modeling and experiment are conducted.

In chapter 2, modeling was established prior to the experiment to determined the effect of the internal heat exchanger and to estimate the expected amount of steam generation. It was found that the effectiveness of the heat exchanger can be simulated by mass flow split ratio and constructed experimentally at next chapter.

In chapter 3, the effect of key variables on the system performance were experimentally investigated. When changing the effectiveness of the internal heat exchanger, changes in evaporation pressure and refrigerant mass flow rate were observed. Also, as mentioned in the previous chapter, the condensing heat converged above the specific effectiveness. Therefore, an optimal mass flow split ratio was observed.

In chapter 4, the dynamic behavior of heat pump with flash tank was identified. Since the internal heat exchanger has a negative effect on the start-up, it is recommended to operate after the flash tank temperature is heated over the heat source temperature. The condensing heat need to be increased by increasing the mass flow rate of the refrigerant to make steam more or higher temperature. Increasing the opening of the expansion valve increases the evaporation temperature, so the limit is set according to the heat source temperature.

Through this study, static and dynamic modeling of the steam generation heat pump were presented and verified by experiments. Although there was modeling for boiler - drum, but dynamic modeling of heat pump – flash tank is an early stage. This study suggested operation measures beyond conventional steady-state studies. In addition, it is proposed that there is a way to change the mass flow rate of the refrigerant in addition to the expansion valve by adjusting the effectiveness of the internal heat exchanger.

References

[1] "The 21th Yearly Session of the Conference of the Parties." United Nations Framework Convention on Climate Change, 2015.

[2] "Estimated U.S. Energy Consumption." Lawrence Livermore National Laboratory, 2018.

[3] "Industrial Energy Efficiency: Using New Technologies to Reduce Energy Use in Industry and Manufacturing." Environmental and Energy Study Institute, 2015.

[4] Andrea, G., Lazini, A., Leone, P., Garcia, M.M.R., Moya, E.Z., "Direct Steam Generation in Parabolic-Trough Collectors: A Review About the Technology and a Thermo-Economic Analysis of a Hybrid System." *Renewable and Sustainable Energy Reviews* 74 (2017): 453-73.

[5] Kim, H.M., Kim, J.H., Cho, H.-H., "Review of Thermal Performance and Efficiency in Evacuated Tube Solar Collector with Various Nanofluids." *International Journal of Air-Conditioning and Refrigeration* 25, no. 02 (2017): 1730001.

[6] KOBELCO, TEPCO (Tokyo electric power corporation), CHUDEN (Chubu electric power corporation), and KEPCO (Kansai electric power corporation). "Steam Generator." 2011.

[7] Kaida, T., Sakuraba, I., Hashimoto, K., Hasegawa, H., "Experimental Performance Evaluation of Heat Pump-Based Steam Supply System." In *IOP Conference Series: Materials Science and Engineering*, 012076,

2015.

[8] Peureux, J-L., Sapora, E., Bobelin, D., "Very High Temperature Heat Pumps Applied to Energy Efficiency in Industry." EDF, 2012.

[9] Lauterbach, C., "Potential, System Analysis and Preliminary Design of Low-Temperature Solar Process Heat Systems." 2014.

[10] Bobelin, D., "Experimental Results of a Newly Developed Very High Temperature Industrial Heat Pump (140°C) Equipped with Scroll Compressors and Working with a New Blend Refrigerant." In *International Refrigeration and Air Conditioning Conference*: Purdue University, 2012.

[11] Miró, L., Brückner, S., Cabeza, L.F., "Mapping and Discussing Industrial Waste Heat (Iwh) Potentials for Different Countries." *Renewable and Sustainable Energy Reviews* 51 (2015): 847-55.

[12] Zhang, J., Zhang, H.-H., He, Y.-L., Tao, W.-Q., "A Comprehensive Review on Advances and Applications of Industrial Heat Pumps Based on the Practices in China." *Applied Energy* 178 (2016): 800-25.

[13] Brückner, S., Liu, S., Miró, L., Radspieler, M., Cabeza, L.F., Lävemann, E., "Industrial Waste Heat Recovery Technologies: An Economic Analysis of Heat Transformation Technologies." *Applied Energy* 151 (2015): 157-67.

[14] Broberg, V., Sarah, Johansson, M.T., "Technologies for Utilization of Industrial Excess Heat: Potentials for Energy Recovery and CO_2

Emission Reduction." *Energy Conversion and Management* 77 (2014): 369-79.

[15] Huang, F., Zheng, J., Baleynaud, J.M., Lu, J., "Heat Recovery Potentials and Technologies in Industrial Zones." *Journal of the Energy Institute* (2016).

[16] "International Energy Agency Heat Pump Technologies." http://heatpumpingtechnologies.org/.

[17] Wang, R.Z., Wang, L.W., Hu, B., L., Jiang, S., Du, Z.Y., Xu, Q.W., Pan. "Refrigerants and Heat Pumps for Efficient Use of Low Grade Thermal Energy." 2017.

[18] Culha, O., Gunerhan, H., Biyik, E., Ekren, O., Hepbasli, A., "Heat Exchanger Applications in Wastewater Source Heat Pumps for Buildings: A Key Review." *Energy and Buildings* 104 (2015): 215-32.

[19] Hepbasli, A., Biyik, E., Ekren, O., Gunerhan, H., Araz, M., "A Key Review of Wastewater Source Heat Pump (Wwshp) Systems." *Energy Conversion and Management* 88 (2014): 700-22.

[20] Xue, B., Iwama, Y., Tanaka, Y., Nakashima, K., Wijayanta, A.T., Nakaso, Fukai, J., "Cyclic Steam Generation from a Novel Zeolite–Water Adsorption Heat Pump Using Low-Grade Waste Heat." *Experimental Thermal and Fluid Science* 46 (2013): 54-63.

[21] Xue, B., Meng, X., Wei, X., Nakaso, K., Fukai, J., "Dynamic Study of Steam Generation from Low-Grade Waste Heat in a Zeolite–Water

Adsorption Heat Pump." *Applied Thermal Engineering* 88 (2015): 451-58.

[22] Liu, F., Sui, J., Liu, H., Jin, H., "Experimental Studies on a Direct-Steam-Generation Absorption Heat Transformer Built with Vertical Falling-Film Heat Exchangers." *Experimental Thermal and Fluid Science* 83 (2017): 9-18.

[23] "Qpinch." https://www.qpinch.com/.

[24] Park, H.S., Kim, M.S., "Performance Analysis of Sequential Carnot Cycles with Finite Heat Sources and Heat Sinks and Its Application in Organic Rankine Cycles." *Energy* 99 (2016): 1-9.

[25] "Ansi/Ashrae Standard 34-2016, Designation and Safety Classification of Refrigerants." https://www.ashrae.org/.

[26] Kim, D.H., Byun, H.W., Yoon, S.H., Song, C.H., Lee, K.H., Kim, O.J., "The Latest Review of Low Gwp (<100) Hfo Refrigerants and Studies on the Pool Boiling Heat Transfer." *International Journal of Air-Conditioning and Refrigeration* 24, no. 04 (2016): 1630009.

[27] Kondou, C., Koyama, S., "Thermodynamic Assessment of High-Temperature Heat Pumps Using Low-Gwp Hfo Refrigerants for Heat Recovery." *International Journal of Refrigeration* 53 (2015): 126-41.

[28] Yu, X., Zhang Y., Na, D., Chen C., Ma, L., Dong, L., Zhang, Y., "Experimental Performance of High Temperature Heat Pump with near-Azeotropic Refrigerant Mixture." *Energy and Buildings* 78 (2014): 43-

49.

[29] Gupta, S., Narasimha, K.K., Ramakrishna, K., Abhishek, D., "Thermodynamic Analysis and Effects of Replacing Hfc by Fourth-Generation Refrigerants in Vcr Systems." *International Journal of Air-Conditioning and Refrigeration* 26, no. 02 (2018): 1850013.

[30] El-Sayed, A.R., Morsi, M.E., Mahmoud, N.A., "A Review of the Potential Replacements of Hcfc/Hfcs Using Environment-Friendly Refrigerants." *International Journal of Air-Conditioning and Refrigeration* 26, no. 03 (2018): 1830002.

[31] Wu, D., Hu, B., Wang, R.Z., "Performance Simulation and Exergy Analysis of a Hybrid Source Heat Pump System with Low Gwp Refrigerants." *Renewable Energy* 116 (2018): 775-85.

[32] Arpagaus, C., Frédéric, B., Michael, U., Schiffmann, J., Bertsch, S.S., "High Temperature Heat Pumps: Market Overview, State of the Art, Research Status, Refrigerants, and Application Potentials." *Energy* 152 (2018): 985-1010.

[33] Yu, X., Zhang, Y., Kong, L., Zhang, Y., "Thermodynamic Analysis and Parameter Estimation of a High-Temperature Industrial Heat Pump Using a New Binary Mixture." *Applied Thermal Engineering* 131 (2018): 715-23.

[34] Fukuda, S., Kondou, C., Takata, N. Koyama, S., 2014, Low GWP refrigerants R1234ze(E) and R1234ze(Z) for high temperature heat

pump, International Journal of Refrigeration, Vol. 40, pp.161-173.

[35] Helminger, F., Hartl, M., Fleckl, T., 2016, Hochtemperatur Warmepumpen Messergebnisse einer Laboranlage mit HFO-1336MZZ-Z bis 160℃ Kondensationstemperatur, 14. Symposium Energieinnovation, TU Graz, p. 1-20.

[36] Nilsson, M., Risla, H.N., Kontomaris, K., 2017, Measured performance of a novel high temperature heat pump with HFO-1336mzz-Z as the working fluid, 12th IEA Heat Pump Conference, p. 1-10.

[37] White, S.D., Yarrall, M.G., Cleland, D.J., Hedley,R.A., "Modelling the Performance of a Transcritical CO_2 Heat Pump for High Temperature Heating." *International Journal of Refrigeration* 25, no. 4 (2002): 479-86.

[38] Bamigbetan, O., Eikevik, T.M., Nekså, P., Bantle, M., "Review of Vapour Compression Heat Pumps for High Temperature Heating Using Natural Working Fluids." *International Journal of Refrigeration* (2017).

[39] Kim, M.S., Lee, J.S., Kim, M.S., "An Experimental Study on the Performance of CO_2 Air-Conditioning Cycle Equipped with an Ejector." International Journal of Air-Conditioning and Refrigeration 17, no. 3 (2009): 100~06.

[40] Chamoun, M., Rulliere, R., Haberschill, P., Berail, J.F., "Dynamic Model of an Industrial Heat Pump Using Water as Refrigerant." International Journal of Refrigeration 35, no. 4 (2012): 1080-91.

[41] Baik, Y.J., Kim, M.-S., Ra, H.-S., "Simulation on the Performance of Carbon Dioxide and Hydrocarbon Heat Pumps for Moderate to High Temperature Heating." International Journal of Air-Conditioning and Refrigeration 22, no. 1 (2013): 8.

[42] Chamoun, M., Rulliere, R., Haberschill, P., Peureux, J.-L., "Modelica-Based Modeling and Simulation of a Twin Screw Compressor for Heat Pump Applications." *Applied Thermal Engineering* 58, no. 1-2 (2013): 479-89.

[43] Chamoun, M., Rulliere, R., Haberschill, P., Peureux, J.-L., "Experimental and Numerical Investigations of a New High Temperature Heat Pump for Industrial Heat Recovery Using Water as Refrigerant." *International Journal of Refrigeration* 44 (2014): 177-88.

[44] Larminat, P., "A High Temperature Heat Pump Using Water Vapor as Working Fluid." Paper presented at the ATMOsphere, Brussels, 2015.

[45] Shen, J., Xing, Z., Zhang, K., He, Z., Wang, X., "Development of a Water-Injected Twin-Screw Compressor for Mechanical Vapor Compression Desalination Systems." *Applied Thermal Engineering* 95 (2016): 125-35.

[46] Bamigbetan, O., Eikevik, T.M., Nekså, P., Bantle, M., Schlemminger, C., "Theoretical Analysis of Suitable Fluids for High Temperature Heat Pumps up to 125 °C Heat Delivery." *International Journal of Refrigeration* 92 (2018): 185-95.

[47] Bamigbetan, O., Eikevik, T.M., Nekså, P., Bantle, M., Schlemminger, C., "The Development of a Hydrocarbon High Temperature Heat Pump for Waste Heat Recovery." *Energy* 173 (2019): 1141-53.

[48] Bobelin, D., Bourig, A., 2012, Experimental results of a newly developed very high temperature industrial heat pump (140°C) equipped with scroll compressors and working with a new blend refrigerant, International Refrigeration and Air Conditioning Conference, Purdue University.

[49] Wolf, S., Fahl, U., Blesl, M., Voss, A., Jakobs, R., 2014, Analyse des Potenzials von Industriewarmepumpen in Deutschland, Forschungsbericht. Universitat Stuttgart, IER.

[50] Wilk, V., Hartl, M., Fleckl, T., Widhalm, E., Ramler, F., Adelberger, G., Ciepiela, T., Ochsner, K., 2016, Hochtemperatur-Wärmepumpe für Industrieanwendungen: Prüfstandsmessungen und Systemsimulation, DKV Tagung, 16-18.

[51] Lee, G.-B., Lee, B.-J., Cho, J.-H., Ra, H.-S., Baik, Y.-J., Ki, S.H., Lee, Y.-S., "Development of Steam Generation Heat Pump through Refrigerant Replacement Approach." In *12th IEA Heat pump conference*. Rotterdam, 2017.

[52] Wang, E.-S., Na, S.-I., Lee, G.-B., Baik, Y.-J., Lee, Y.-S., Lee, B,-J., "Experimental Study on Heating Performance Characteristic of 100 Kw Heat Pump to Generate 120℃ Steam." *Korean Journal of Air-Conditioning and Refrigeration Engineering* 30, no. 2 (2018): 100-06.

[53] Kang, D.H., Na, S.-I., Kim, M.S., "Recent Researches on Steam Generation Heat Pump System." *International Journal of Air-Conditioning and Refrigeration* 25, no. 04 (2017).

[54] Jogwar, S.S., Daoutidis, P., "Dynamics and Control of Vapor Recompression Distillation." *Journal of Process Control* 19, no. 10 (2009): 1737-50.

[55] Zhou, Y., Shi, C., Dong, G., "Analysis of a Mechanical Vapor Recompression Wastewater Distillation System." *Desalination* 353 (2014): 91-97.

[56] Onishi, V.C., Alba C.-P., Juan A.R.-L., Rubén R.-F., Raquel S.-D., Eric S.F., José A.C., "Shale Gas Flowback Water Desalination: Single Vs Multiple-Effect Evaporation with Vapor Recompression Cycle and Thermal Integration." *Desalination* 404 (2017): 230-48.

[57] Dong, H., "Study on Zero-Emission Desalination System Based on Mechanical Vapor Recompression Technology." *Energy Procedia* 75 (2015): 1436-44.

[58] Walmsley, T.G., Atkins, M.J., Walmsley, M.R.W., Neale, J.R., "Appropriate Placement of Vapour Recompression in Ultra-Low Energy Industrial Milk Evaporation Systems Using Pinch Analysis." *Energy* 116 (2016): 1269-81.

[59] Kazemi, A., Hosseini, M., Arjomand, M.-Z., Faizi, V., "Evaluation of Different Vapor Recompression Distillation Configurations Based on

Energy Requirements and Associated Costs." *Applied Thermal Engineering* 94 (2016): 305-13.

[60] Bless, F., Arpagaus, C., Bertsch, S.S., Schiffmann, J., "Theoretical Analysis of Steam Generation Methods - Energy, Co 2 Emission, and Cost Analysis." *Energy* 129 (2017): 114-21.

[61] Lee, J.H., 2018, “Study on the Performance of Steam Generation Heat Pump using Waste Heat Source with Suction Line/Liquid Line Heat Exchanger,” Seoul National University

[62] Yan, Y.-Y., Lio, H.-C., Lin, T.-F., 1999, Condensation heat transfer and pressure drop of refrigerant R-134a in a plate heat exchanger, International journal of heat and mass transfer, Vol.42, pp. 993-1006

[63] Yan, Y.-Y., Lin, T.-F., 1999, Evaporation heat transfer and pressure drop of refrigerant R-134a in a plate heat exchanger, Transaction of the ASME, Vol.121

[64] Estefanía, H.-B., Pitarch, M., Emilio N.avarro-Peris, and José M. Corberán. "Optimal Sizing of a Heat Pump Booster for Sanitary Hot Water Production to Maximize Benefit for the Substitution of Gas Boilers." Energy 127 (2017): 558-70.

[65] Oh, S.H., Lee, G.B., Lee, B.J., Ra, H.-S., Cho, J.-H., Baik, Y.-J., Lee, Y.-S., 2016, A study on reliability evaluation test of compressor for high temperature heat-pump based on gas bypass cycle, Korean Society of Mechanical Engineers – Thermal Engineering Division Spring

Conference, pp. 326-327.

[66] Lemmon, E., Huber, M., McLinden, M., 2018, NIST Standard Reference Database 23: Reference Fluid Thermodynamic and Transport Properties - REFPROP, Version 10.0. National Institute of Standards and Technology, Gaithersburg, MD, U.S.A.

[67] ASHRAE Guideline 2, 2010, Engineering analysis of experimental data, ASHRAE, Atlanta, Georgia.

[68] Kim, M.S., Kang, D.H., Kim, M.S., Kim, M., 2017, Investigation on the optimal control of gas cooler pressure for a CO_2 refrigeration system with an internal heat exchanger, International Journal of Refrigeration, Vol.77, pp. 48-59.

[69] Bahadori, A., Vuthaluru, H.B., "A Method for Estimation of Recoverable Heat from Blowdown Systems During Steam Generation." Energy 35, no. 8 (2010): 3501-07.

[70] Zhou, Y., Wang, D., "An Improved Coordinated Control Technology for Coal-Fired Boiler-Turbine Plant Based on Flexible Steam Extraction System." Applied Thermal Engineering 125 (2017): 1047-60.

[71] Chandrasekharan, S., Panda, R.C., Bhuvaneswari, N.S., "Mathematical Model for Integrated Coal Fired Thermal Boiler Using Physical Laws." Energy 118 (2017): 985-98.

[72] Chandrasekharan, S., Panda, R.C., Swaminathan, B.N, Panda, A., "Operational Control of an Integrated Drum Boiler of a Coal Fired

Thermal Power Plant." Energy 159 (2018): 977-87.

[73] Sunil, P. U., Barve, J., Natarajm, P.S.V., "Mathematical Modeling, Simulation and Validation of a Boiler Drum: Some Investigations." Energy 126 (2017): 312-25.

[74] Sunil, P. U., Barve, J., Nataraj, P.S.V., "A Robust Heat Recovery Steam Generator Drum Level Control for Wide Range Operation Flexibility Considering Renewable Energy Integration." Energy 163 (2018): 873-93.

[75] Harish, S., Baldi, S., "Monitoring Energy Efficiency of Condensing Boilers Via Hybrid First-Principle Modelling and Estimation." Energy 142 (2018): 121-29.

[76] Sedić, A., Katulić, S., Pavković, D., "Dynamic Model of a Natural Water Circulation Boiler Suitable for on-Line Monitoring of Fossil/Alternative Fuel Plants." Energy Conversion and Management 87 (2014): 1248-60.

[77] Liu, J.-Z., Yan, S., Zeng, D.L., Hu, Y., Lv, Y., "A Dynamic Model Used for Controller Design of a Coal Fired Once-through Boiler-Turbine Unit." Energy 93 (2015): 2069-78.

[78] Tognoli, M., Najafi, B., Rinaldi, F., "Dynamic Modelling and Optimal Sizing of Industrial Fire-Tube Boilers for Various Demand Profiles." Applied Thermal Engineering 132 (2018): 341-51.

[79] Beyne, W., Lecompte, S., Ameel, B., Daenens, D., Belleghem, M.V., Paepe, M.D., "Dynamic and Steady State Performance Model of Fire Tube Boilers with Different Turn Boxes." Applied Thermal Engineering

149 (2019): 1454-62.

[80] Sanaye, S., Chahartaghi, M., Asgari, H., "Dynamic Modeling of Gas Engine Driven Heat Pump System in Cooling Mode." Energy 55 (2013): 195-208.

[81] Koury, R.N.N., Faria, R.N., Nunes, R.O., Ismail, K.A.R., Machado, L., "Dynamic Model and Experimental Study of an Air–Water Heat Pump for Residential Use." International Journal of Refrigeration 36, no. 3 (2013): 674-88.

[82] Faria, R.N., Nunes, R.O., Koury, R.N.N., Machado, L., "Dynamic Modeling Study for a Solar Evaporator with Expansion Valve Assembly of a Transcritical Co 2 Heat Pump." International Journal of Refrigeration 64 (2016): 203-13.

[83] Qiao, H., Aute, V., Radermacher, R., "Dynamic Modeling and Characteristic Analysis of a Two-Stage Vapor Injection Heat Pump System under Frosting Conditions." International Journal of Refrigeration 84 (2017): 181-97.

[84] Liu, F., Zhu, W., Zhao, J., "Model-Based Dynamic Optimal Control of a CO_2 Heat Pump Coupled with Hot and Cold Thermal Storages." Applied Thermal Engineering 128 (2018): 1116-25.

[85] Deutz, K.R., Charles, G.L., Cauret, O., Rullière, R., Haberschill, P., "Detailed and Dynamic Variable Speed Air Source Heat Pump Water Heater Model: Combining a Zonal Tank Model Approach with a Grey

Box Heat Pump Model." International Journal of Refrigeration 92 (2018): 55-69.

[86] Yearbook of energy statics, KEEI (Korea Energy Economics Institute), 2018

[87] Industrial combustion boilers, IEA (International energy agency) ETSAP (Energy technology systems analysis programme) Technology Brief, May 2010

[88] Kang, D.H., Na, S.-I., Yoo, J.W., Lee J.H., Kim, M.S., "Experimental study on the performance of a steam generation heat pump with the internal heat exchanging effect." International Journal of Refrigeration 108 (2019): 154-162

국 문 초 록

지구 온난화로 인한 국제적인 환경 협약으로 인해 에너지 소비량의 저감이 필요한 시점이다. 이 중 제조업 중심 국가일수록 산업부문이 에너지 소비량의 큰 비중을 차지하며, 그 중에서도 스팀 생산이 큰 비중을 차지한다. 스팀 생산과 동시에 방류 전 냉각이 필요한 미 활용 열 또한 회수할 수 있는 수단으로써 히트 펌프를 도입하는 것이 최근 고려되고 있다. 임계 온도가 높은 신 냉매들의 등장으로 기존의 산업용, 가정용 온수 생산을 넘어 스팀 생산이 가능해졌기 때문이다. 히트 펌프는 초기 투입된 연료 에너지에 대비하여 많은 열 생산 및 저온 열원의 회수가 가능하다.

하지만 100도 이상의 고온부를 가져 스팀을 만들 수 있는 히트 펌프에 대한 연구는 현재까지 많이 진행되어 있지 않은 상황이다. 기존의 연구들은 높은 온도에서 작동 가능한 냉매의 종류 탐색과 시스템 구성 간의 비교 연구 등이 진행되었다. 시스템 구성으로는 내부 열교환기의 적용이 높은 성능을 보이고 있다. 하지만, 내부 열교환기의 구성의 변경에 대한 연구와, 실제 스팀을 만들기 위한 플래시탱크가 접목된 연구는 제한적이다.

이에 따라 본 연구에서는 스팀 생산 히트 펌프의 일반적으로 예상되는 운전 조건을 고려하여, 에너지 효율을 높이는 방향으로 설계 및 동적 특성을 파악하고자 하였다. 이를 위해 해석적 연구를 실험에 선행하여 내부 열교환기의 구성 변경을 모사할 방안을 탐색하고, 실험적 연구를 진행하였다.

실험을 통하여 스팀 생산 히트 펌프의 성능 향상의 방향을 제시하였고, 각 제어 변수와 온도와 유체 유량이 난방 용량 및 성능계수에 미치는 영향을 분석하였다. 히트 펌프에 바이패스 배관을 이

용하여 내부 열교환기의 유량을 변경시켰고, 구성요소 별 열 용량 및 냉매 질량유량이 변경되는 것을 관찰하였다. 이는 팽창밸브 외에도 증발 압력과 냉매 질량유량을 변경할 한 수단이 될 수 있으며, 후 스팀 수요의 변경에 따라 히트펌프의 거동을 변경하게 되어 에너지 소비의 저감을 이룰 것이 기대된다.

또한 기존에 대기압에서도 가능하던 온수 생산과 달리, 증기의 생산을 위해서는 물의 상을 분리하는 고압의 플래시 탱크가 도입되는데, 스팀의 생산량과 탱크의 압력이 히트 펌프의 거동에도 밀접하게 영향을 미치게 된다. 장치의 시동 과정에서 투입되는 물의 온도가 열원 온도보다 상승하기까지, 물이 끓기 시작하기까지, 플래시 탱크의 압력이 일정해지기까지의 거동 별로 그 특성이 모두 다르다. 이에 따라 본 연구에서는 시동 조건에서 히트 펌프가 고려된 플래시 탱크의 동적 특성 변화를 해석적으로 연구하여 모델을 제시하였고, 이를 실험 결과와 대비하였다.

이와 같은 연구를 통해 추후 플래시 탱크가 연동된 고온의 스팀 생산 히트 펌프의 연구에서 거동을 해석함에 도움이 될 것으로 기대되며, 에너지 소비의 저감을 이룰 것이 기대된다.

주요어: 히트 펌프, 플래시 탱크, 스팀 생산, 내부 열 교환, 미 활용 열, 열 회수, 동적 특성

학 번: 2014-21570